Porphyry Cu-Au and epithermal deposits:
Srednogorie Zone (Bulgaria) Macedonia

Pb-Zn deposits
Rhodope Massif (Laki, Madna)

IGP excursion 2015

Madan vein deposits

Organised by:
A. von Quadt & Th. Driesner (ETH Zurich)
I. Peytcheva (BAS)
N. Georgiev (BAS)
I. Gerdijov (Uni St.K.)
St. Georgiev (Uni St. K.)
R. Vasseliva (BAS)
BAS: Bulgarian Academy of Science
Uni St. K.: St. Kliment Ohridski University Sofia

Elatisite porphyryr Cu-Au-PGE deposit

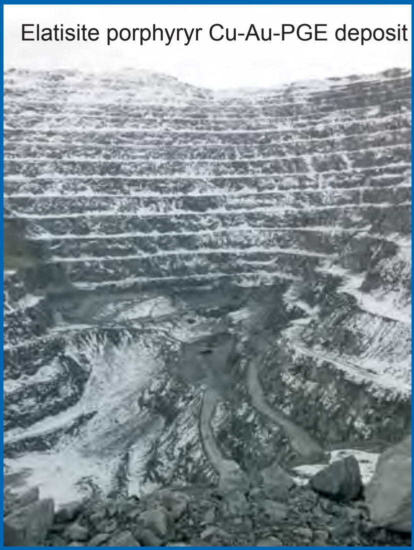

31. May - 13. June 2015

Edited by
Albrecht von Quadt, Thomas Driesner & Irena Peytcheva
Department of Earth Sciences, Institute of Geochemistry and Petrology (IGP)
ETH Zurich, Clausiusstrasse 25, CH-8092 Zurich, Switzerland

Rila monastery

Melnik

page

Content

PARTICIPANTS

Akker, Vénice
D-ERDW – Department of Earth Science, ETH Zurich,
Sonneggstrasse 5, CH-8092 Zürich
Tel: +
e-mail: veniceakker@gmail.com

Argapadmi, Windeati
D-ERDW – Department of Earth Science, ETH Zurich,
Sonneggstrasse 5, CH-8092 Zürich
Tel: +
e-mail: argapadw@student.ethz.ch

Balashova, Anna
D-ERDW – Department of Earth Science, ETH Zurich,
Sonneggstrasse 5, CH-8092 Zürich
Tel: +
e-mail: anna.balashova@erdw.ethz.ch

Bircher, Christian
D-ERDW – Department of Earth Science, ETH Zurich,
Sonneggstrasse 5, CH-8092 Zürich
Tel: +
e-mail: cbircher@student.ethz.ch

Fiedrich, Alina
D-ERDW – Department of Earth Science, ETH Zurich,
Sonneggstrasse 5, CH-8092 Zürich
Tel: +
e-mail: falina@student.ethz.ch

Frøystein, Maria
D-ERDW – Department of Earth Science, ETH Zurich,
Sonneggstrasse 5, CH-8092 Zürich
Tel: +
e-mail: marf90@gmail.com

Gies, Hannah
D-ERDW – Department of Earth Science, ETH Zurich,
Sonneggstrasse 5, CH-8092 Zürich
Tel: +
e-mail: hgies@student.ethz.ch

Hsu, Ying-Jui [Ingrid]
D-ERDW – Department of Earth Science, ETH Zurich,
Sonneggstrasse 5, CH-8092 Zürich
Tel: +
e-mail: ying-jui.hsu@erdw.ethz.ch

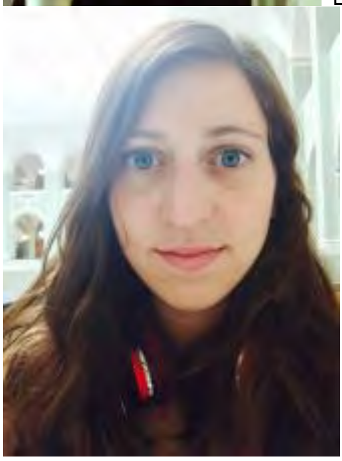

Keusch, Rebecca
D-ERDW – Department of Earth Science, ETH Zurich,
Sonneggstrasse 5, CH-8092 Zürich
Tel: +
e-mail: rekeusch@student.ethz.ch

Klimentyeva, Dina
D-ERDW – Department of Earth Science, ETH Zurich,
Sonneggstrasse 5, CH-8092 Zürich
Tel: +
e-mail: kdina@student.ethz.ch

Kolly, Alban
D-ERDW – Department of Earth Science, ETH Zurich,
Sonneggstrasse 5, CH-8092 Zürich
Tel: +
e-mail: kollyal@student.ethz.ch

Large, Simon
D-ERDW – Department of Earth Science, ETH Zurich,
Sonneggstrasse 5, CH-8092 Zürich
Tel: +
e-mail: simon.large@erdw.ethz.ch

Leisibach, Elena
D-ERDW – Department of Earth Science, ETH Zurich,
Sonneggstrasse 5, CH-8092 Zürich
Tel: +
e-mail: elenal@student.ethz.ch

Reger, Philip
D-ERDW – Department of Earth Science, ETH Zurich,
Sonneggstrasse 5, CH-8092 Zürich
Tel: +
e-mail: regerp@student.ethz.ch

Roozen, Stan
D-ERDW – Department of Earth Science, ETH Zurich,
Sonneggstrasse 5, CH-8092 Zürich
Tel: +
e-mail: stanroozen@gmail.com

De Schaetzen, Caroline
D-ERDW – Department of Earth Science, ETH Zurich,
Sonneggstrasse 5, CH-8092 Zürich
Tel: +
e-mail: deschaec@student.ethz.ch

Dinev, Lasen
Sofia University "St. Kliment Ohridski"
Faculty of Geology and Geography, 1504 Sofia, 15 Tsar Osvoboditel Blvd.

Kynev, Silvestar
Sofia University "St. Kliment Ohridski"
Faculty of Geology and Geography, 1504 Sofia, 15 Tsar Osvoboditel Blvd.

Georgieva, Gabriela
Sofia University "St. Kliment Ohridski"
Faculty of Geology and Geography, 1504 Sofia, 15 Tsar Osvoboditel Blvd.

Petrov, Georgi
Sofia University "St. Kliment Ohridski"
Faculty of Geology and Geography, 1504 Sofia, 15 Tsar Osvoboditel Blvd.

Chavdarova, Silvia
Sofia University "St. Kliment Ohridski"
Faculty of Geology and Geography, 1504 Sofia, 15 Tsar Osvoboditel Blvd.

Pantelic, Nemanja
University of Belgrade, Faculty of Mining and Geology,
Tel: +
e-mail: nemanja.pantelic@rgf.rs

Bosic, Dragana
University of Belgrade, Faculty of Mining and Geology,
Tel: +
e-mail: dragana.bosic@yahoo.com

Georgiev, Neven
Sofia University “St. Kliment Ohridski”
Faculty of Geology and Geography, 1504 Sofia, 15 Tsar Osvoboditel Blvd.
e-mail: neven@gea.uni-sofia.bg

Vaseliva, Rositza
BAS – Bulgarian Academy of Science, Geological Institute, Acad. G. Bonchev st. bl 24, 1113 Sofia, Bulgaria
e-mail: rosivas@geology.bas.bg

Georgiev, Stoyan
BAS – Bulgarian Academy of Science, Geological Institute, Acad. G. Bonchev st. bl 24, 1113 Sofia, Bulgaria
e-mail: stoyang@geology.bas.bg

Gerdijov, Ianko
Sofia University “St. Kliment Ohridski”
Faculty of Geology and Geography, 1504 Sofia, 15 Tsar Osvoboditel Blvd.
e-mail: @gea.uni-sofia.bg

Peytcheva, Irena
BAS – Bulgarian Academy of Science, Geological Institute, Acad. G. Bonchev st. bl 24, 1113 Sofia,
D-ERDW – Department of Earth Science, ETH Zurich, Sonneggstrasse 5, CH-8092 Zürich
Tel: +
mail: peytcheva@erdw.ethz.ch

Driesner, Thomas
D-ERDW – Department of Earth Science, ETH Zurich,
IGP, Clausiusstrasse 5, CH-8092 Zürich
Tel: +
e-mail: thomas.driesner@erdw.ethz.ch

Von Quadt, Albrecht
D-ERDW – Department of Earth Science,
ETH Zurich, IGP, Clausiusstrasse 25, CH-8092 Zürich
Tel: +
e-mail: vonquadt@erdw.ethz.ch

Excursion in BG – 31.05.-13.06.2015

1.	31.05.2015	Arrival in Sofia – Sofia – Etropole - Pravets	80 km	S
2.	01.06.2015	Pravets – Elatzite – occurrences around - Koprivshtitsa	40 km	M
3.	02.06.2015	Koprivshtitsa – Chelopech – Vozdol – Panagyurishte	80 km	T
4.	03.06.2015	Panagyurishte – Asarel – Petrich - Panagyurishte	70 km	W
5.	04.06.2015	Panagyurishte – Boshulya/Vetren – Dolna banja – Melnik	250 km	T
6.	05.06.2015	Melnik – Ilovitsa (FYRMaacedonia) – Melnik	150 km	F
7.	06.06.2015	Melnik – Gotze Delchev – Pamporovo (with geological stops)	150 km	S
8.	07.06.2015	Pamporovo – Madan – Pamporovo	60 km	S
9.	08.06.2015	Pamporovo – Laki – Pamporovo	150 km	M
10.	09.06.2015	Pamporovo - Krumovgrad – Ada Tepe – Krumovgrad (+geol)	40 km	T
11.	10.06.2015	Krumovgrad – Nanovitsa - Perperikon – Sozopol - Kiten	180 km	W
12.	11.06.2015	Kiten – Volcanics in E Srednogorie – Kiten	40 km	T
13.	12.06.2015	Kiten – Chernomorets – Sofia (cult. stops in Plovdiv, Starosel?)	500 km	S
14.	13.06.2015	roundtrip Sofia? Departure	30 km	S

Around 2000 km

Chernomorets
Kiten
Elatsite
Chelopech
Asarel
Pamporovo
Laki
Madan
Ada Tepe

Hannah Gies & Elena Leisibach

Tectonical and Geological view of the Srednogorie

The Srednogorie zone is part of the Alpine–Balkan-Carpathian–Dinaride belt (ABCD) which is a segment of the Alpine–Himalayan orogenic system (see figure 1). This belt extents almost 1500 km from Eastern Europe to Central Europe. More specifically, the area is located in the L-shaped ABTS belt (Apuseni-Banat-Timok-Srednogorie), an extensive zone of calc-alkaline magmatism, and is one of the oldest known mining areas for Cu and Au. Geographically, the Srednogorie zone is located in Bulgaria and spreads from around 400 km west from Sofia until Burgas next to the Black Sea with a width of about 200 km. Important active mines in the Panagyurishte district are Elatsite, Chelopech, and Assarel.

Tectonics

The ABCD belt resulted from the plate convergence of Africa and Europe in the past 180 Ma. From paleomagnetic data of Willingshofer (2000), the plate configuration from the late Cretaceous was reconstructed. The units are divided into the ALCAPA (**AL**pine-**CA**rpathian-**PA**nnonian) block, the Tisia block, the Dacia block, the Rhodope block and the south – Alpine Dinaric block (see Figure 2). The ALCAPA block comprises the Austroalpine units from Eastern Alps and inner Western Carpathians, the Tisia block reaches from Zagreb to the Apuseni Mountains, Romania, the Dacia block includes Eastern and Southern Carpathians and the Balkan. (von Quadt et al., 2005) The collision of the ALCAPA, Tisia and Dacia blocks resulted in an EW trending orogeny at 80Ma which correlates with the occurence of strong in the ABCTS belt (see figure 2). Reconstructions indicate the presence of open ocean basins to the north and south of the orogenic belt. The orogeny was connected either by subduction or collision, which process of both is not yet entirely clear, to the Moesian Platform to the east and to the Adriatic Microplate to the west (Neubauer, 2002). Magmatism in the Srednogorie zone is related to a back arc tectonic setting (Boccaletti et al., 1978), as the Tethys Ocean was subducted northwards underneath the southern margin of Europe for about 100 Ma (Wortel and Spakmann, 2000). The generated magma formed mainly by dehydration of the slab and was proposed to be enhanced by upwelling of the asthenosphere and orogenic parallel extension (Neubauer, 2002).

Geology

Intrusive as well as extrusive products of calc-alkaline magmatism during the late cretaceous characterize the Srednogorie zone and the other parts of the ABTS-belt, however, the rocks found in the Srednogorie are relatively mafic. Calc-alkaline and peralkaline rocks with gabbroic/basaltic to granitic/rhyolitic composition are abundant in the eastern Srednogorie, across the belt a zonation from calc-alkaline in the south to shoshonitic and potassic alkaline in the north was observed. The central Srednogorie is predominated by intermediate rocks as andesites, diorites and monzodiorites (von Quadt et al., 2005). Over the whole belt, a younging trend from north to south is observable. Strontium and Neodymium isotope analysis of the rocks revealed a mixed crust and mantle origin or melted juvenile crust, the trace element pattern suggests volcanic arc-related as well as destructive continental margin magmatism, which is coherent with the proposed tectonical setting of the Srednogorie zone (von Quadt et al., 2005). The late cretaceous rocks overly a basement of magmatic orthogneisses, paragneisses and amphibolites from the Paleozoic covered by Permian and Triassic sedimentary rocks. The metamorphic grade of the basement increases weakly towards the south of the Srednogorie (Velichkova et al., 2004)

Deposits

The Panagyurishte district, a N-NW-oriented corridor 55-95km east from Sofia covering an area of 1500km^2 in the Central Srednogorie (Popov et al., 2003) is of special interest, as it is one of the two distinct regions in the ABTS-belt, that comprise economic ore bodies, primarily porphyry copper and massive sulphide deposits (Heinrich&Neubauer, 2002). Up to today 95% of the Bulgarian copper and gold production originate from this area (von Quadt et al., 2005).

The calc-alkaline to alkaline magmatic rocks of the late cretaceous cover highly metamorphosed basement rocks, two mica gneisses, mica schists, ortho-amphibolites, serpentinite bodies and anatexites, from the Lower Paleozoic called the Srednogorie type metamorphic unit (von Quadt et al., 2005). In the northernmost parts of the district the rocks were only subject to lower grade metamorphism, they are part of the Berkovitsa group, which consists of a Lower Paleozoic volcanic-sedimentary sequence.

The products of Late Cretaceous alkaline to calc-alkaline magmatism vary across the Panagyrishte corridor: effusive andesitic rocks predominate in the northern part of the district, whereas the southern part is characterized by holocrystalline plutonic rocks with a granodioritic composition. Rhyolites and rhyodacites are restricted to the southern and central part of the district. Porphyry copper deposits are generally found in subvolcanic dacite, quartz-monzodiorite and granodiorite intrusions, which were derived from the same magma as the Late Cretaceous volcanic rocks (see figure 3). U-Pb-dating revealed that the magmatic activity in the Panagyurishte corridor covered a time span of only 14 million years with a younging trend from north to south as observed also in other parts of the Srednogorie zone, however, each hydrothermally mineralized deposits were found to have a life time of approximately 1 million years or less (von Quadt et al., 2005). The profitability of the deposits is closely related to the age of the magmatic rocks: huge deposits are located in the northern older part of the corridor, the tonnage decreases towards the south of the Panagyurishte district, the youngest intrusions in the southernmost area do not host any ore deposits at all (von Quadt et al., 2005).

Why all deposits are aligned is still not entirely resolved, however, researchers suspect a zone of weakness, for example transverse structures in the basement rocks (von Quadt et al., 2005; Heinrich&Neubauer, 2002).

References:

Boccaletti, M., Manetti, P., Peccerillo, A., Stanisheva-Vassileva, G., 1978. Late Cretaceous high-potassium volcanism in eastern Srednogorie, Bulgaria. Geological Society of America Bulletin 89, 439–447.

Heinrich, C.A., Neubauer, F., 2002. Cu–Au–Pb–Zn–Ag metallo- geny of the Alpine–Balkan–Carpathian–Dinaride geodynamic province. Mineralium Deposita 37, 533–540.

Neubauer, F., 2002. Contrasting Late Cretaceous with Neogene ore provinces in the Alpine–Balkan–Carpathian–Dinaride collision belt. In: Blundell, D.J., Neubauer, F., von Quadt, A. (Eds.), The Timing and Location of Major Ore Deposits in an Evolving Orogen, Geological Society, London, Special Publications no. 204, pp. 81–102.

Popov, P., Strashimirov, S., Popov, K., Petrunov, R., Kanazirski, M., Tsonev, D., 2003. Main features in geology and metallogeny of the Panagyurishte ore region. 50 Years University of Mining and Geology bSt Ivan RilskiQ, Annual Volume 46, 119–125.

Schmid, S. M., Bernoulli, D., Fügenschuh, B., Matenco, L., Schefer, S., Schuster, R., ... & Ustaszewski, K., 2008. The Alpine-Carpathian-Dinaridic orogenic system: correlation and evolution of tectonic units. Swiss Journal of Geosciences, *101*(1), 139-183.

Velichkova, S. H., Handler, R., Neubauer, F., & Ivanov, Z., 2004. Variscan to Alpine tectonothermal evolution of the Central Srednogorie unit, Bulgaria: constraints from 40Ar/39Ar analysis. Swiss Bulletin of Mineralogy and Petrology, *84*(1), 133-151.

von Quadt, A., Moritz, R., Peytcheva, I., & Heinrich, C. A. ,2005. 3: Geochronology and geodynamics of Late Cretaceous magmatism and Cu–Au mineralization in the Panagyurishte region of the Apuseni–Banat–Timok–Srednogorie belt, Bulgaria. Ore Geology Reviews, 27(1), 95-126.

Willingshofer, E., 2000. Extension in collisional orogenic belts: the Late Cretaceous evolution of the Alps and Carpathians. Ph.D. thesis, Vrije Universiteit, Amsterdam, 146 pp.

Wortel, M.J.R., Spakman, W., 2000. Subduction and slab detach- ment in the Mediterranean–Carpathian region. Science 290, 1910 – 1917.

Appendix

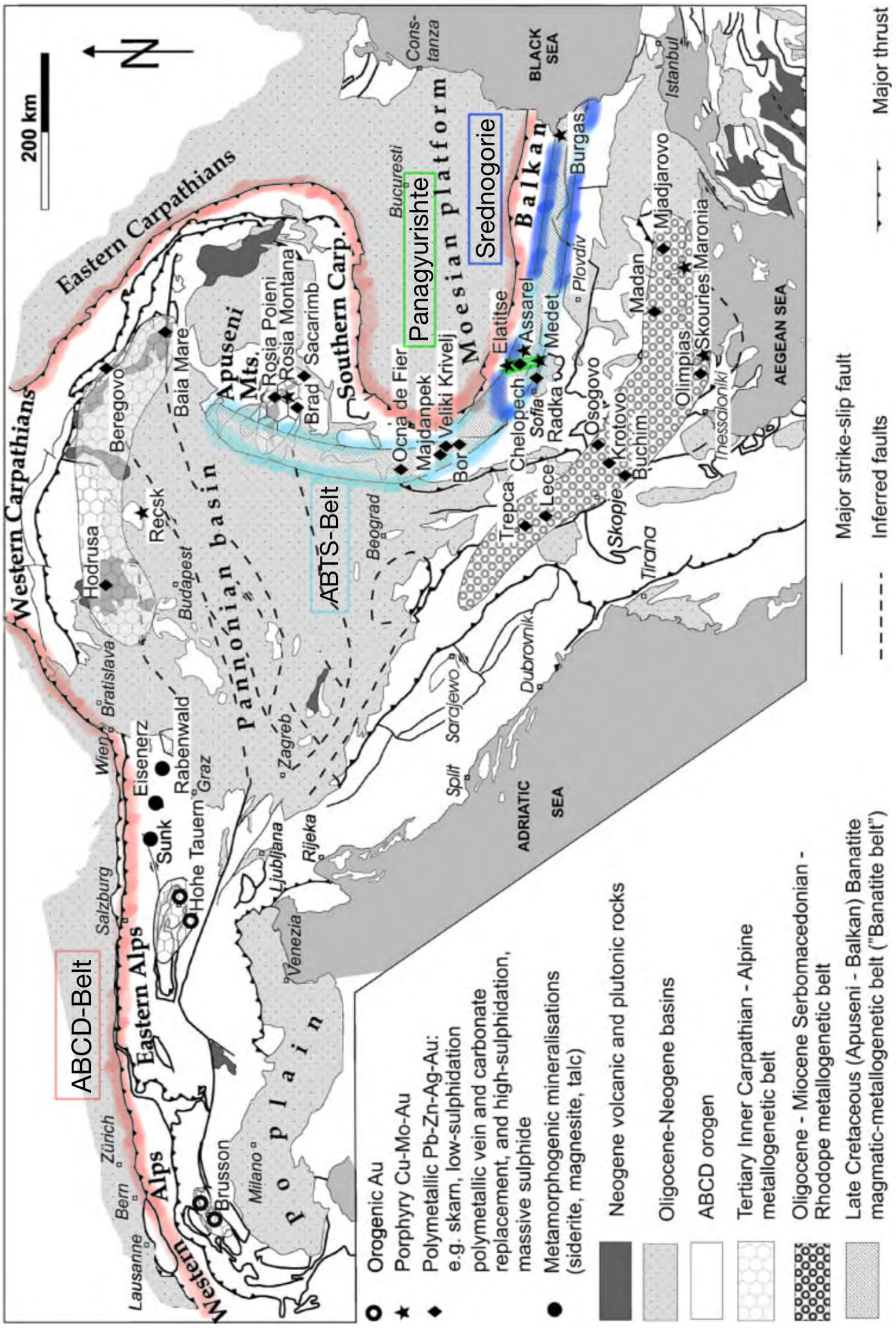

Figure 1: Map of the ABCD - belt and the ABTS - belt (Heinrich&Neubauer, 2002)

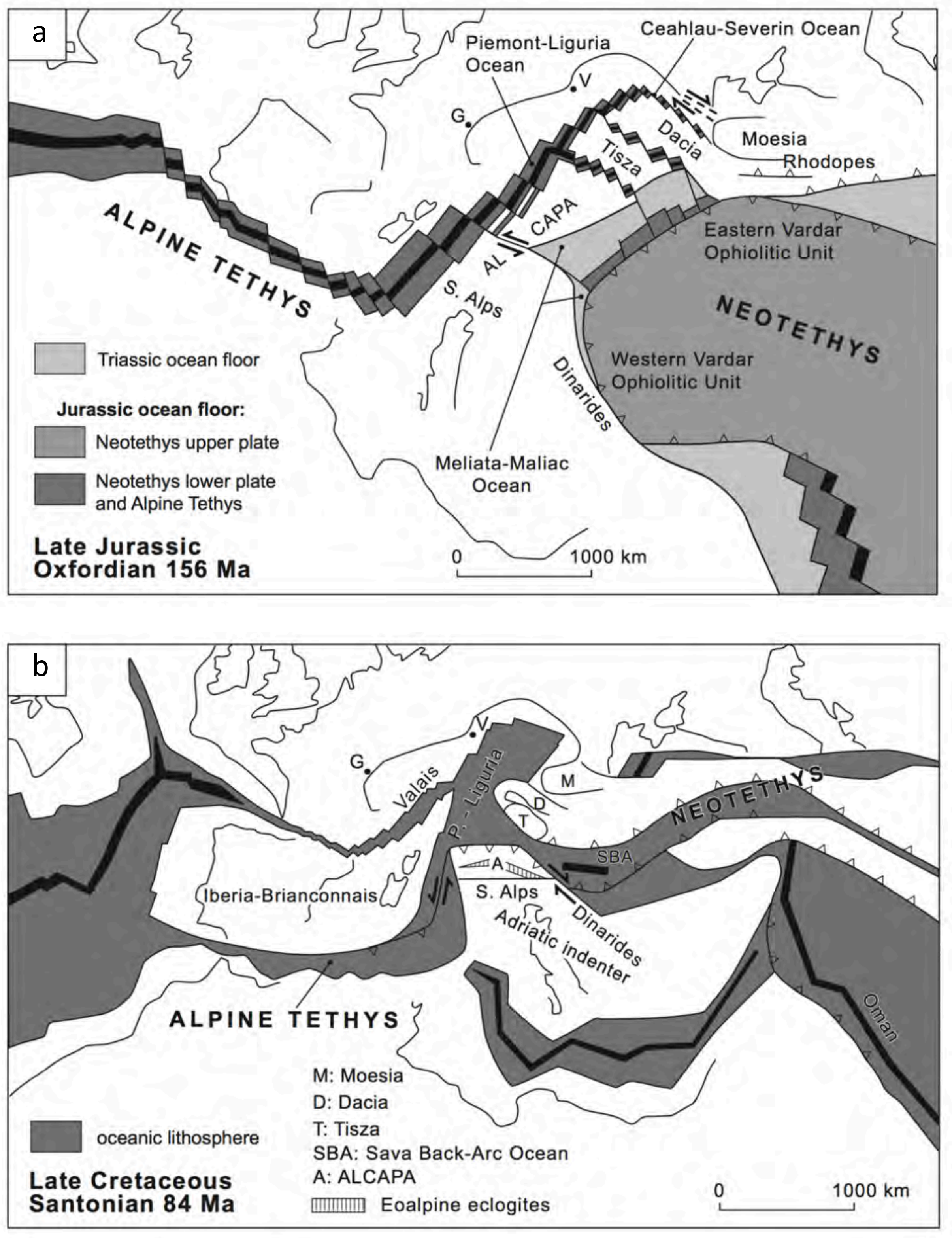

Figure 2: Paleographic setting of the orogeny during the late Jurassic (a) and the late Cretaceous (b) (Schmid et al., 2008)

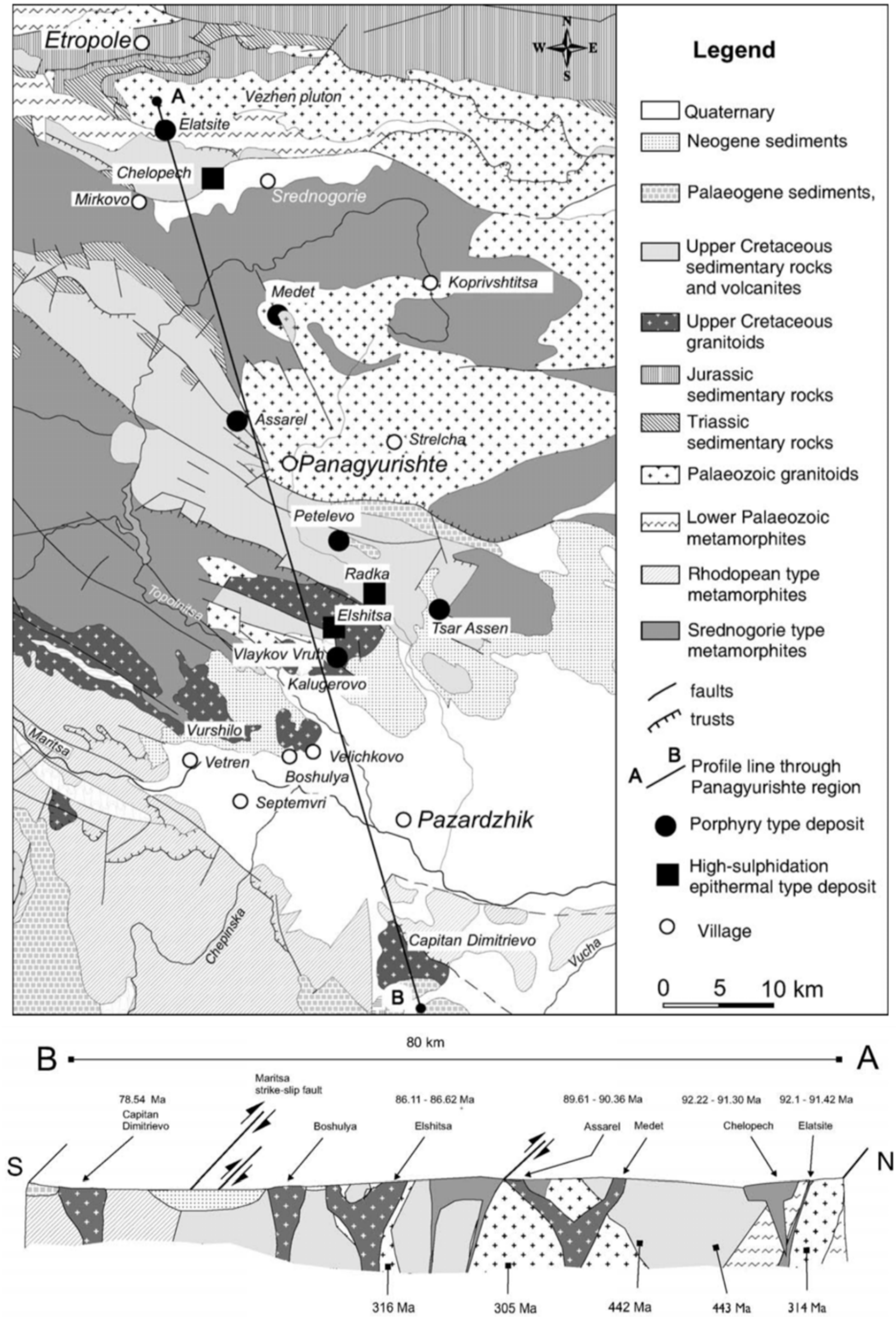

Figure 3: Geological map of the Panagyurishte corridor showing important ore deposits with transect (von Quadt et. al, 2005)

Elatsite Cu-Au Porphyry

Introduction

The Elatsite porphyry is part of Srednogorie volcanic-plutonic zone, which probably is an upper Cretaceous, calc-alkaline, island arc. The Srednogorie zone is situated in the Alpine-Balkan-Carpathian-Dinaride metallogenic province fig. 1. (Kehayov et al., 2003)

The Elatsite porphyry is located in Bulgaria, 50 km northeast of Sofia and 15 km south of Etropole. It is a copper mine, with Gold as by-product. It is operated since 1980. The Elatsite mine is estimated to have a reserve of 650 million tonnes of ore, with a grade of ~0.3% of copper. In 2010, 178 thousand tonnes of copper concentrate have been produced. The size of the ore body is approximately 1000m x 700m. The mine is owned by Geotechmin group. (http://www.geotechmin.com/en/pages/ellatzite-med-8.html, 16.5.2015)

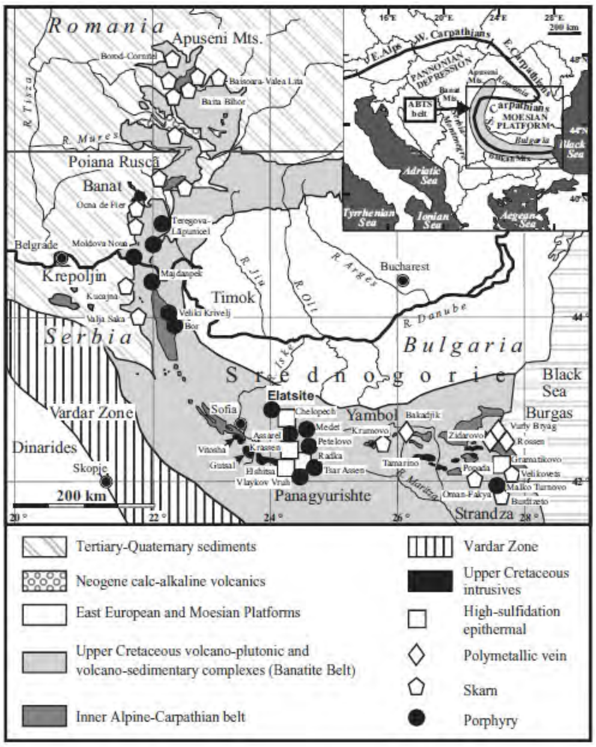

Figure 4 Geological map of Bulgaria

Geology

Rocks

The oldest lithology in the Elatsite mine is a Sericite-Phyllite (greenschist phyllites, low metamorphosed basalts, and marbles) of Precambrian-Cambrian age.
Those got intruded by a Granodiorite (Vezhen pluton) in the middle of the Carboniferous. This intrusion generated a contact metamorphose, that can be seen as Biotite-Hornfels. The metamorphosed zone was three to four hundred meters wide, but faulting and brittle-to-ductile deformation overprinted it. Rocks from Permian to Jurassic age cannot be found in the mine.
In upper Cretaceous times the Srednogorie zone formed. Fluids originating from calk-alkaline magmas ran through Elatsite. This intrusion has generated at least seven generations of dykes (diorites and monzodiorites). As accessory mineral magnetite can be found. The porphyry stock work is linked to these cretaceous subvolcanic intrusions (Fig. 2; Fanger, 2001).

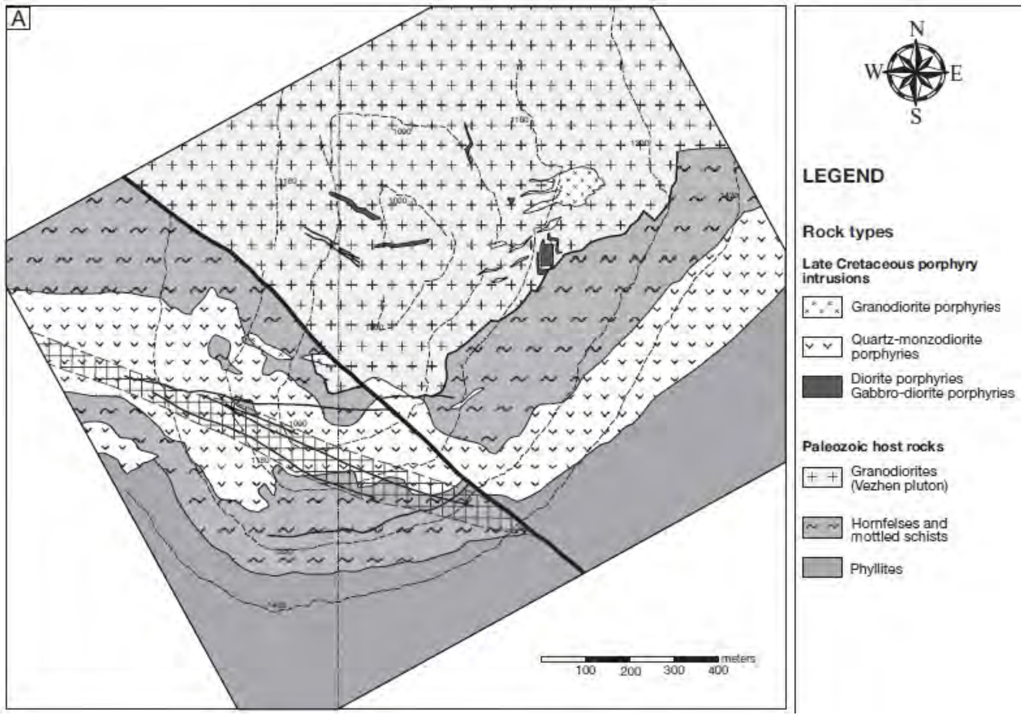

Figure 5: Geological map of the Elatsite mine

Time relations

Clear timings relations were found by combining the crosscutting relationships between dykes and magmatic-hydrothermal veins with silicate melt inclusions, fluid inclusions and ore mineralization. These all show that the ore minerals all deposited late in the evolution of the porphyry system at moderate temperatures of about 200-300 degree Celsius (Kehayov et al., 2003). This is later and at lower temperatures then usually is found in similar kind of systems; there it is more commonly found during the interaction of magmatic dykes and veining near magmatic temperatures at about 600 degrees Celsius. (Stefanova et al., 2013)

Dikes and Veins

In this paragraph we will go step for step through the evolution of the Porphyry system of Elatsite. At first there were the monzodioritic porphyry dykes. Veining started with quartz magnetite veins and further fluids derived from the dykes gave rise to abundant granular quartz veining. This veining was accompanied by some potassic alteration. Then a second granodioritic dyke swarm intruded the system that on itself again gave rise to a second generation of granular quartz veining with potassic alteration fig. 3. Some more open spaced versions of these granular quartz veins also show injections of aplitic material. This aplitic material is interpreted to be hydrous residual melts that were

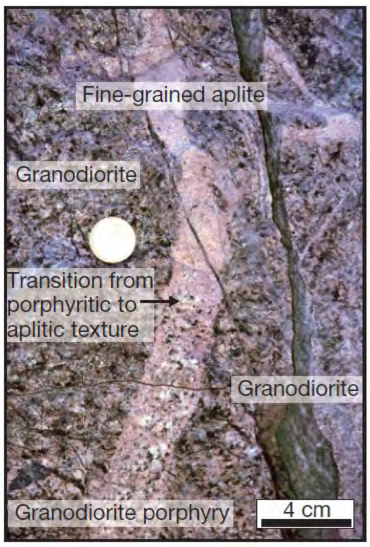

Figure 6 Example of dykes in Elatsite

expelled from the granodioritic dykes. These same aplitic melt also occur as small melt inclusions in lot of the later granular quartz veins. Fluid inclusion found in the above described veins are all of intermediate density and have more or less 8 wt% NaCl and where most probably trapped under near lithostatic conditions at a depth of about 4-5 km at about 730 degree Celsius. Phase separation into a brine and a vapour phase seems to have happened at that same time at 2-3 km depth at lower temperatures of about 600 degrees. (Stefanova et al., 2013).

Ore mineralization

Ore mineralization seems to have started with the quartz-bornite-chalcopyrite-magnetite veining and was again accompanied with potassic alteration. These ore minerals deposited from a lower temperature fluid of about 460 degree Celsius and at about a kilometre depth (hot hydrostatic regime). Local dissolution of quartz must have taken place upon further cooling of the system so that it passed through the window of retrograde quartz solubility. The later and economically most imported veining lacks quartz precipitation and therefore also fluid inclusions so until now it is unsure at which exact pressure and temperature these ore deposits formed. They mostly postdate the potassic alteration and present themselves mostly as veins without any gangue minerals in planar fractures. The late quartz-pyrite veining postdates the economic mineralization and is associated with intensive seritic alteration and either develops as massive veins or as dissemination in the host rocks in the marginal part of the porphyry system. Later Mafic dykes and quartz diorite porphyries are found rarely at Elatsite but more frequent in the surroundings. Last but not least some veining seems to have occurred in the last stages of the porphyry system evolution with the precipitation of a quartz-carbonate-zeolite veins that must have precipitated from a fluid at very low temperatures of about 145 degree Celsius as indicated by the fluid inclusions. (Stefanova et al., 2013)

Very high Cu concentrations where measured in the intermediate density fluid and the early vapour phases. In vapour inclusions just before the ore deposition however this concentration falls down rapidly. As this happens at the same time as anhydrite inclusions start to form. This might indicate that the driving force for the partitioning of the Cu into the brine phase occurred because of a general lack of sulphur in the vapour phase. Alternatively the later vapour fluid inclusions were not affected by later enrichment of Cu after the inclusion already had formed.

The progressive trend in the grade of Cu mineralization that is found in Elatsite is an indicator that depressurization might have played an important role to the mineralization process. Taking into account mass balance considerations it is likely that the brine part was of minor importance and therefore most likely stayed down maybe ripping off the Cu of the vapour phase while it came by. So the history of the porphyry copper system can be summarized as the following:

1. Monzodioritic dyke (D1)

2. Granular quartz veining with potassic alteration (Fluid inc: salty, near magmatic T and 4-5 km depth) (V1)
3. Granodioritic dyke intrusions (D2)
4. Granular quartz veining with potassic alterations (Fluid inc: salty, near magmatic T and 4-5 km depth), fluid separation at 3-4 km depth at 630 degree (V2)
5. quartz-bornite-chalcopyrite-magnetite veining with potassic alteration at 460 degree Celsius and 260 to 325 bars (V3)
6. Local dissolution of quartz
7. Economic ore veining without quartz (V3)
8. quartz-pyrite veining and seritic alteration (V3)
9. Mafic dykes and Quartz diorite dykes
10. Quartz-carbonate-zeolite veining at 145 degree Celsius.

(Stefanova et al, 2013)

Age

Precise U-Pb zircon geochronology showed that the first monzodioritic dyke has an age of approximately 92.1+-0.3 Ma. Zircon of the latest granodioritic dyke that cut the main ore mineral veining showed ages of 91.84+- 0.3 Ma. So ore forming magmatism and associated hydrothermal processes cannot have been longer than 1.1 Ma and have most probably even a much shorter lifespan.
Geochemical discrimination ratios suggest that the source of the magma is mix between mantle and crustal magma's during the Late Cretaceous. Isotope analysis of Sr, Nd and Hf also confirm that the deposit originate form an enriched magma source with crustal contamination that could explain the moderately radiogenic Pb. (von Quadt et al., 2002)

References:

Kehayov,R., Bogdanov,K., Fanger L, Quadt A., Pettke T, Heinrich C.2003. The Fluid chemical evolution of the Elatsite porphyry Cu-Au-PGE Deposit, Bulgaria. 7th Biennial SGA meeting "Mineral Exploration and Sustainable Development" August 24–28, Athens, Greece, Abs. Vol., Eliopoulos et al. (eds), p. 1173 – 1176.

von Quadt, A., Peytcheva, I., Kamenov, B., Fanger, - L., Heinrich, C.A. and Frank, M. (2002): The Elatsite porphyry copper deposit in the Panagyurishte ore district, Srednogorie zone, Bulgaria:; U-Pb zircon geochronology and isotope-geochemical investigations of magmatism and ore genesis. In: Blundell, D.J., Neubauer, F. and Von Quadt, A. (eds), The timing and location of major ore deposits in an evolving orogen. Geol. Soc. London, Spec. Publication 204, p. 81-102.

Stefanova E, Driesner T, Zajacz Z, Heinrich CA, Petrov P, Zlati V (2013) Melt and fluid inclusions in hydrothermal veins: The magmatic to hydrothermal evolution of the Elatsite porphyry Cu-Au deposit, Bulgaria. Economic Geology, in press.

L. Fanger, 2001. Geology of a porphyry copper (-Au-PGE) ore deposit: Elatsite, Bulgaria. MSc Thesis. ETHZ: Switzerland

High-Sulfidation Cu-Au Chelopech deposit

Introduction

The Chelopech high-sulfidation epithermal deposit is located about 60 km east of Sofia in the NNW trending Panagyurishte ore district, Bulgaria, containing several Upper Cretaceous porphyry Cu hosted by intrusions and locally volcanic and country rocks and epithermal Cu-Au deposits hosted by volcanic and sedimentary rocks (Fig. 1). The Panagyurishte ore district is part of the Apuseni-Banat-Timok-Srednogorie belt (ABTS-belt) extending from the Bulgarian Black Sea coast all the way to Serbia and further on to Romania. The Chelopech deposit is the largest European gold deposit, and the mine is owned by the Canadian-based mining company Dundee Precious Metals Inc. In 2013 the company produced about 20’000 tonnes of copper and 3.7 tonnes of gold. Proven and probable reserves are estimated to be around 22 megatonnes of ore, with ore grades of 1.4% for copper and 3.6 g/t for gold making it comparable in size to Cenozoic world-class deposits in the circum-pacific region.

Panagyurishte ore district:

The ABTS-belt is part of the Alpine-Balkan-Carpathian orogeny that resulted from the convergence between Africa and Europe and the closure of the Tethyan ocean since the Cretaceous (Chamberfort and Moritz, 2007). In Bulgaria the E-W trending Srednogorie zone is located between the northern Balkan Zone and the Rhodope massif and Sakar-Strandja Zone in the south (Fig. 1). The Panagyurishte ore district hosting a number of mined or previously mined deposits (e.g. Chelopech and Elatsite) is located in the central Srednogorie zone about 60 – 90 km east of Sofia. The deposits are aligned on a NNW oriented trend that is oblique to the large E-W trending Srednogorie zone (Chamberfort and Moritz, 2006).
Some of the major operating European gold and base metal deposits are located in the ABTS-belt (like the deposits in the Panagyurishte district or in the Timok district) and it is one of the main areas of exploration in Europe with recent, exciting discoveries. Most of the ore deposits in the belt are the result of subduction-related magmatism during the plate convergence (Chamberfort and Moritz, 2006).

The Chelopech high-sulfidation epithermal Cu-Au deposit

The orebodies of the deposit are hosted by a subvolcanic body of andesitic composition and associated with a phreatomagmatic breccia and by sedimentary rocks interbedded with a volcanic tuff (Fig. 2). Alteration at the deposit is characterised by an innermost silicic zone with massive silica and rare vuggy silica zoning out into a quartz-kaolonite-dickite zone a widespread quartz-sericite zone and an outer propylitic zone (Chamberfort and Moritz, 2006; Chamberfort et al, 2007). The mineralization underwent three stages during ore formation: The first stage is

Fe-S pyrite-markasite mineralization, with massive pyrite deposits found in volcanic tuffs and sedimentary rock layers. The second stage is the gold-bearing Cu-As-S stage, the part of the deposit that is economic for mining. Minerals present are luzonite (Cu_3AsS_4), enargite (Cu_3AsS_4), tennantite ($(Cu,Fe)_{12}As_4S_{13}$), bomite (Cu_5FeS_4) as well as native gold. The third stage are uneconomic galena and sphalerite veins (Chamberfort and Moritz, 2006; Chamberfort et al, 2007).
The main Chelopech deposit has two satellite ore bodies: The Charlodere occurrence about 1 km NE of the mine and the polymetallic Vozdol prospect NNE of the mine.
U-Pb ages of the hydrothermally altered rocks (91.45 +/- 0.15 Ma) and of a later breccia containing altered clasts allows for determining a time range of where the Chelopech alteration may have occurred. Within uncertainty, it is shown that the alteration took place between 91.6 Ma and 91.0 Ma, lasting for 600'000 years at the longest (Chamberfort et al., 2007).

Lithology:
The basement rocks consist of different metamorphic rocks of Precambrian to Cambiran age and Paleozoic magmatic rocks that all underwent ductile deformation and low-grade metamorphism around 100 Ma ago. The basement is unconformably overlain by Turonian sediments. These early sedimentary rocks are cut and overlain by Upper Cretaceous intrusive and extrusive rocks, whereby subvolcanic and effusive rocks are dominant in the northern part of the Pangayursihte district and intrusive rocks dominate in the southern part, possibly indicating higher erosion levels in the southern part. The volcanic rocks are interbedded with sedimentary rocks containing abundant volcanic rock fragments, that are possibly the result of destabilisation of the volcanic edifice. The interbedded sequences are overlain by younger a transgressive sedimentary sequence. Flysch units deposited as outer-fan lobe are credited for the preservation of the volcanic rocks from erosion in the northern part of the district (Chamberfort and Moritz, 2006).

Evolution of magma bodies
Three different units of volcanic deposits can be distinguished in the Chelopech complex: (1) Dome-like bodies extruded through underlying sediments and the metamorphic basement. The dome rocks are of andesitic and trachydacitic composition, highly porphyric with >40% phenocrysts of mainly plagioclase and zoned amphiboles with minor biotite, titanite and corroded quartz crystals. The microlitic texture consists of plagioclase and amphiboles exclusively. Accessory minerals are apatite, zircon and Ti-magnetite. (2) Lava and agglomerate flows of latitic-trachy-dacitic to dacitic compositions. The phenocrysts, microlites and accessory minerals are the same as those in the first unit, minus the corroded quartz. Basaltic andesite and shoshonite enclaves are found in the lava flows, indicating magma mingling and mixing. (3) So-called Vozdol volcanic breccias and

volcanites. These deposits are the youngest and final stage of magmatic activity in the region, as they intersect the other volcanic units. Sedimentary lenses as well as more large-scale intercalations and covers of (most likely contemporary) sedimentary material with the basaltic andesitic to latitic Vozdol unit are wide-spread, but more common towards the edges of the magmatic body. Phenocrysts are less common than in the other two units. The first two units are more felsic than the third unit (61-64 wt% SiO2 versus 56-58wt% SiO2). The volcanic deposits are covered by resedimented volcanoclastic rocks, as well as sedimentary rocks from the Late Cretaceous, the Paleogene and the Neogene (Stoykov et al, 2004).
U-Pb zircon geochronology gives us concordant ages of 92.2 +/- 0.3 Ma for the first unit, interpreted as the time of intrusion of the andesitic body, with the regression line of the data points pointing to a discordant age of 467 +/- 28 Ma. The mean U-Pb ages for both the second and third units are 91.3 +/- 0.3 Ma. Geochemical analyses of Nd and Sr isotopes as well as rare earth and trace element patterns show typical characteristics for subduction-related volcanism and provide indications of a mixed mantle-crust origin for the magma throughout the Chelopech volcanic complex, however, Hf isotopic ratios of the oldest zircons in the dome-like bodies of the first unit show possible assimilation of the magma in the upper crust, though the magma evolution could also be principally due to magma mingling and mixing (Stoykov et al, 2004; Chamberfort et al, 2007).

Magma source comparison between Chelopech and Elatsite

The Elatsite porphyry copper deposit is situated about six kilometers to the NW of Chelopech and porphyry Cu and high suflidation epithermal Cu-Au deposits in the Banat-Timok-Srednogorie belt generally show a spatial association. And magmatism has a generally calk-alkaline composition suggesting an island arc or continental arc setting. The Elattsite porphyry copper deposit has been reported to have formed at 92.10 +/- 0.30 Ma and 91.84 +/- 0.31 Ma, making it an older deposit than the Chelopech high-sulfidation deposit. This is in accordance with a regional north to south younging direction of magmatism in the region. Hafnium isotopes analysis help reveal that the Elatsite and the Chelopech deposit may have had different magma sources: a mixed crustal-mantle source for Chelopech, while a mostly mantle source is derived in the case of Elatsite deposit. This suggest that two distinct intrusions coexisted in the region 91 – 92 Myrs ago. (Chamberfort et al, 2007)

Tectonic and Geodynamic evolution of the Panagyurishte ore district and the Chelopech deposit:

The Chelopech deposit has three characteristic fault sets with the orientations ~N55, ~N110 and ~N155 termed F1, F2 and F3, respectively by Chamberfort and Moritz (2006). The F1 fault set is characterised by thrust or reverse faults varying in orientation between N20 and N55 and dipping about 40 to 50° to the south. They are

often associated with post-volcanic folds. The F2 fault set consists of strike-slip faults oriented between N90 and N110 (sub parallel to the Srednogorie belt) with a subvertical to 60° dip to the south. F3 faults are strike-slip faults oriented between N135 and N170 (subparallel to the ore deposit alignment in the Pnagyurishte district) with a vertical to 60° dip. The F1 and F2 fault sets are clearly associated with the ore-forming event as the long axis of the orebodies, the breccias and the silicified zones are subparallel to the fault orientations.
All fault sets existed prior to ore formation and have been reactivated several times with all of them being active during ore formation and all of them showing post-ore movement during which the ore-body was also tilted. However, the the chronology of the different fault sets could not be reconstructed by Chamberfort and Moritz (2006). The complete rock package deposited in the Late Cretaceous in the Pangyurishte ore district underwent folding resulting in WNW trending folds. This was followed by overthrusting of older rocks over the Late Cretaceous rock package along the F1 reverse faults. The deposited and intruded rock suite before ore deposition indicates an extensional setting. The later folding indicates a compressional regime. Therefore, the Chelopech deposit formed during the transformation from an extensional to compressional setting as has been described for several other preserved epithermal deposits (Chamberfort and Moritz, 2006).
As the other high-sulfidation epithermal deposits and associated magmatic rocks in the area are also controlled by the F1 and F2 fault sets and as they are all located on an alignment of the same orientation as the F3 fault set the deposits in the Panagyurishte district were most likely formed under in a similar tectonic environment and similar stress conditions (Fig. 3; Chamberfort and Moritz, 2006). Combining theses observations with the progressive younging of the magmatic rocks in the district to the south the geodynamic situation during ore-formation is most likely the result of slab rollback for about 14 Ma.

References:

Chambefort, I., & Moritz, R. (2006). Late Cretaceous structural control and Alpine overprint of the high-sulfidation Cu–Au epithermal Chelopech deposit, Srednogorie belt, Bulgaria. *Mineralium Deposita*, *41*(3), 259-280.

Chambefort, I., Moritz, R., & von Quadt, A. (2007). Petrology, geochemistry and U–Pb geochronology of magmatic rocks from the high-sulfidation epithermal Au–Cu Chelopech deposit, Srednogorie zone, Bulgaria. *Mineralium Deposita*, *42*(7), 665-690.

Stoykov, S., Peytcheva, I., Von Quadt, A., Moritz, R., Frank, M., & Fontignie, D. (2004). Timing and magma evolution of the Chelopech volcanic complex (Bulgaria). *Swiss Bulletin of Mineralogy and Petrology*, *84*(1), 101-117.

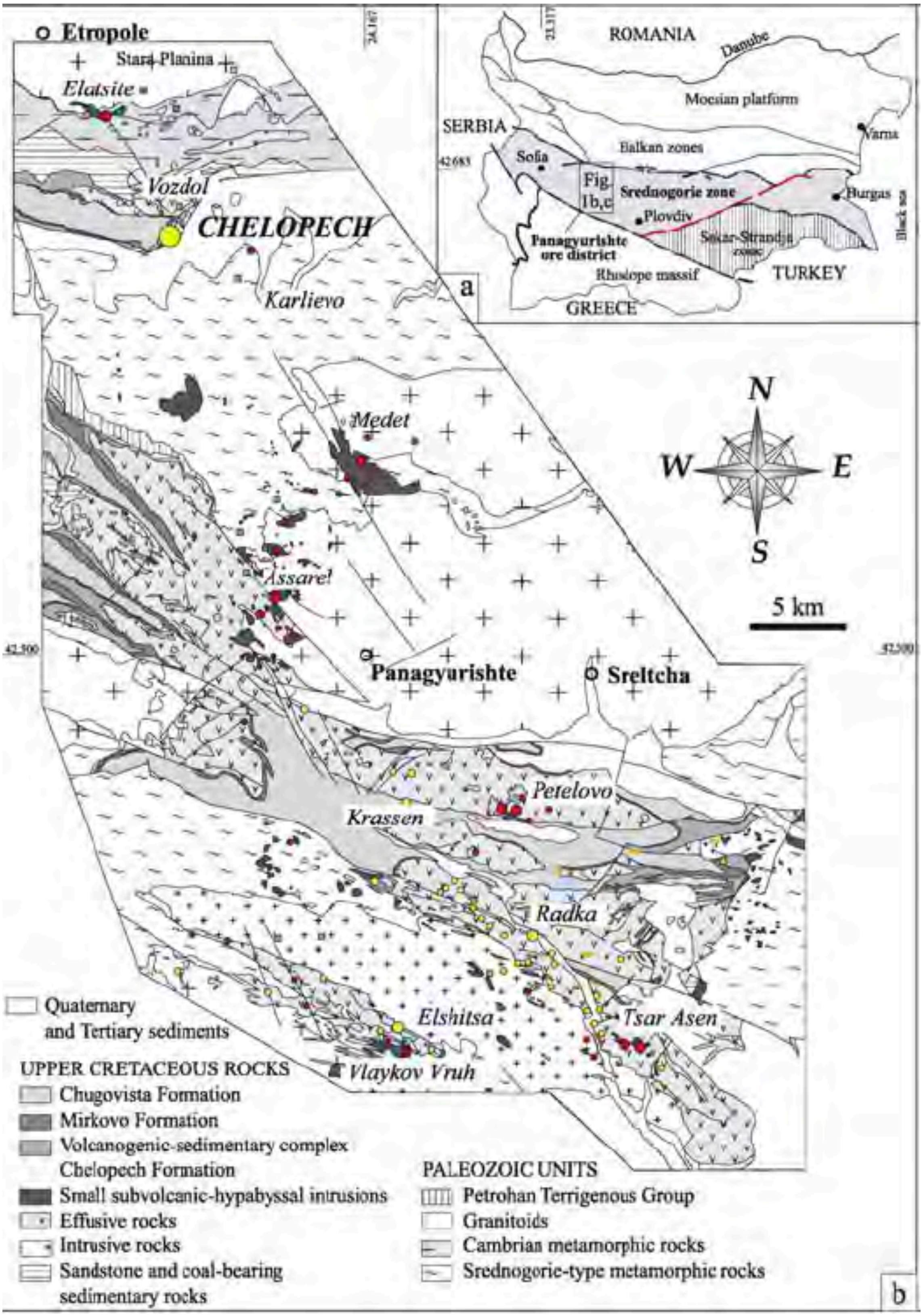

Figure 1: a) Major tectonic zones of Bulgaria, b) The Panagyurishte ore district with different deposits from Chamberfort and Moritz (2006).

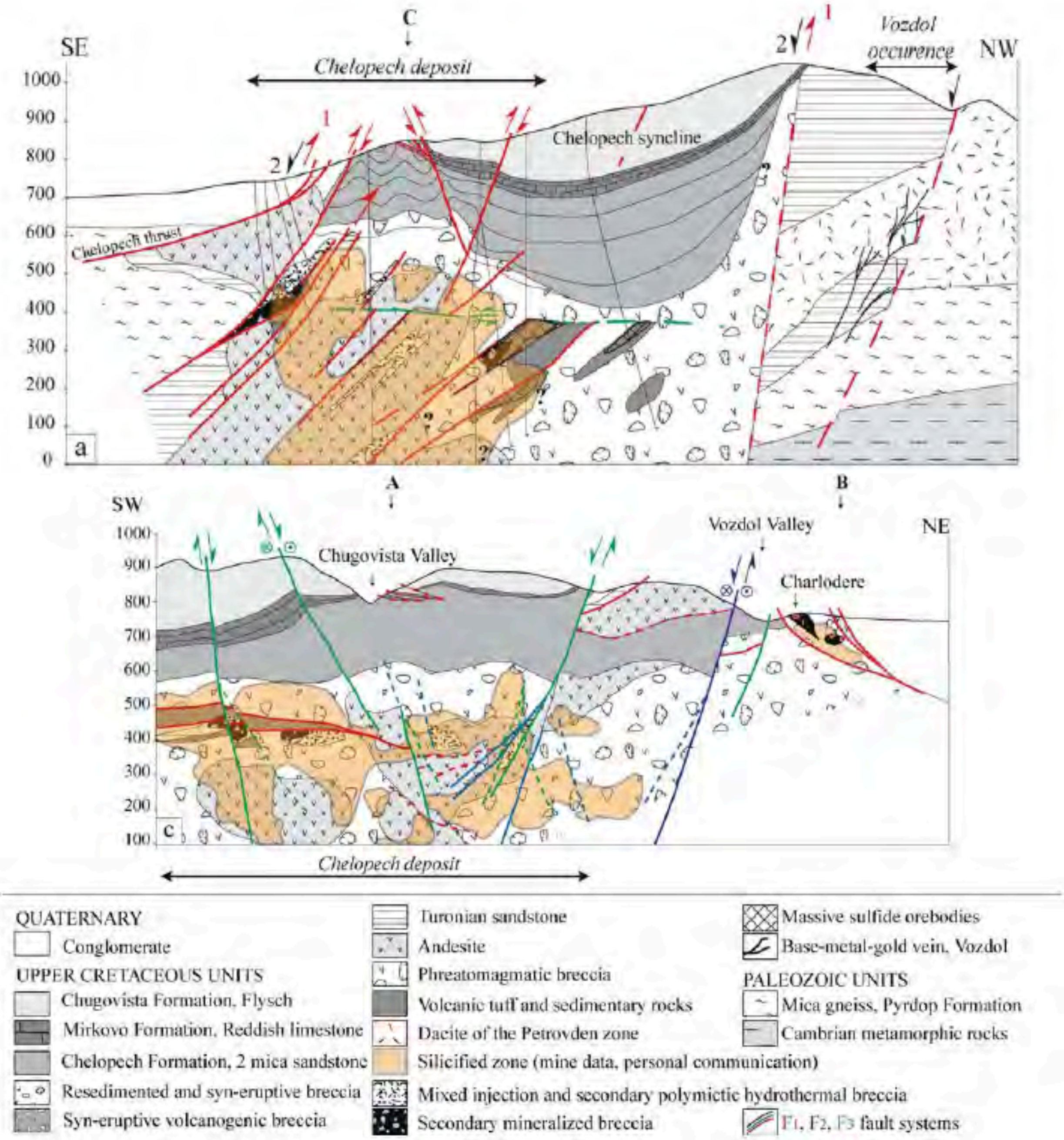

Figure 2: Cross-sections through the Chelopech deposit from Chamberfort and Moritz (2006). A) Is perpendicular to the direction of F1 and B) is perpendicular to F3.

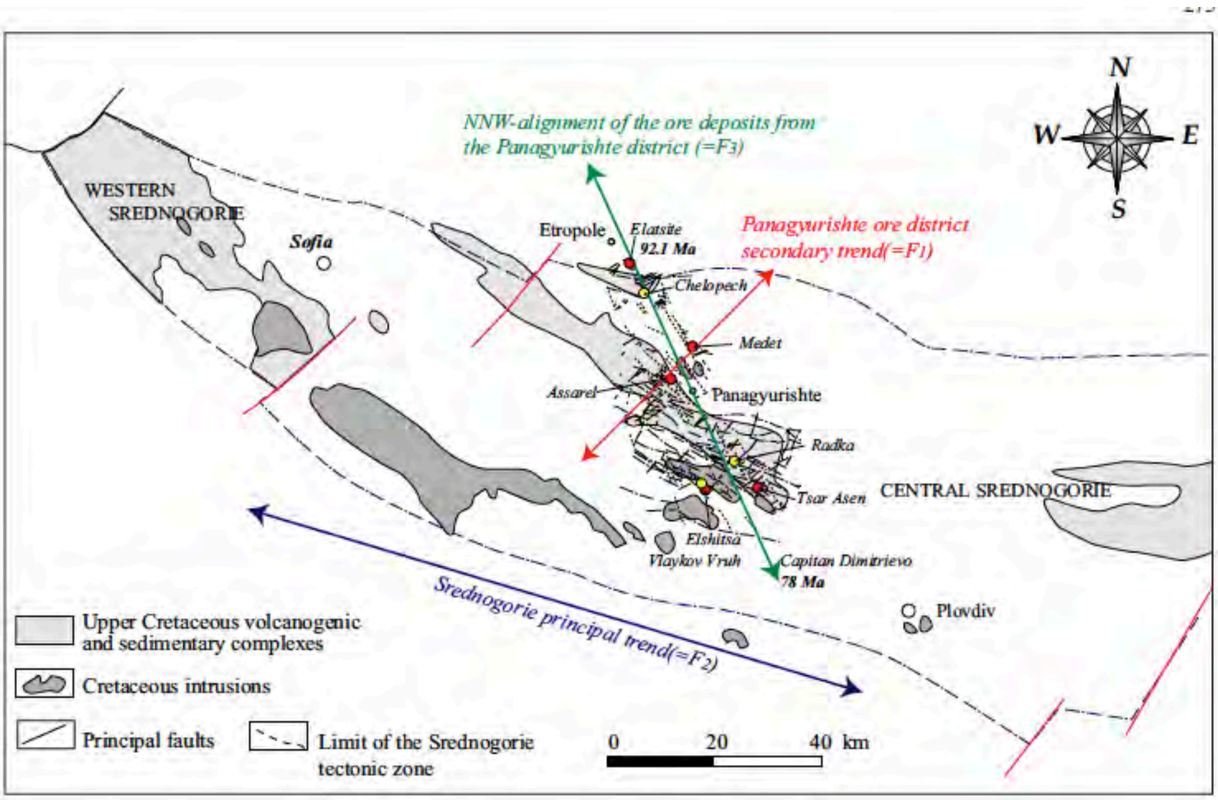

Figure 3: View of the Srednogorie belt with main fault orientations from Chamberfort and Moritz (2006).

Medet and Assarel lithocap-secondary enrichment

Medet and Assarel are known as porphyry copper deposits in Bulgaria. These deposits are located in Panagyurishte region, which is around 70 km ESE from the capital, Sofia. This region is situated in the central part of Srenogorie tectonic zone, which is part of the Apuseni-Banat-Timok-Srednogorie (ABTS) belt, an elongated Late Cretaceous belt of Eastern Europe (Figure 1).

There are 163 Mt of ore have been mined from Medet within the period of 1964-1993, with average grade of 0.32% of Cu and 0.1 g/t of Au. Meanwhile in Assarel, the production reached 350 Mt starting from 1976, with average grade of 0.44% Cu and Au as byproduct (Strashimirov et al., 2002).

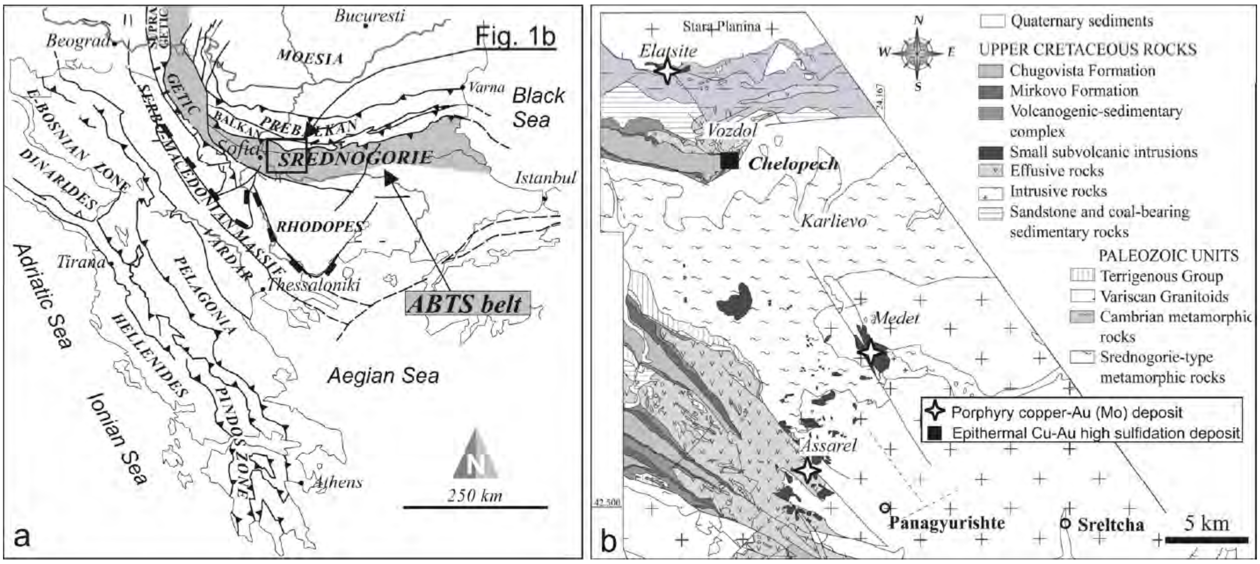

Figure 1: (a) Tectonic map of the Balkan peninsula with the position of ABTS belt; (b) Geological map of the northern part of Central Srednogorie (from Peytcheva et al., 2007 modified after Popov & Popov, 2000).

Medet Geology and Mineralization

The Medet porphyry copper deposit is hosted by quartz-monzodiorite and granodiorite that intruded the Assarel-Medet ore field (Figure 2). The basement are Paleozoic granites and metamorphic rocks. The published age of the quartz monzodiorite (Peytcheva et al. 2007) revealed that the fertile magmatism were active since 90.59 ± 0.29 Ma then was accomplished at 89.26 ± 0.32 Ma, the time of the post-ore granodiorite porphyry dyke. The two main alteration types in the Medet porphyry deposit are K-silicate and propylitic alteration (Ushev et al., 1962). The K-silicate alteration mainly consist of K-feldspar, biotite, quartz, and apatite. The propylitc alteration assemblage is chlorite, epidote, and carbonate. The sulfide mineralization took place within the propylitic alteration zone accompanied with

sericite alteration. The sulfides are pyrite and chalcopyrite.
Strashimirov et al. (2003) made a compilation of ore mineral zonation of the Medet porphyry copper deposit. The first ore mineral assemblage is quartz-magnetite-hematite±bornite±chalcopyrite associated with K-silicate ± propylitic alteration type. This assemblage also contain Ti-bearing minerals such as ilmenite and rutile. The main pervasive quartz-pyrite-chalcopyrite, occur as dissemination and veinlets. This assemblage in Medet is associated with gold, Co-Ni,- and Bi-Ag-Te-bearing minerals. The quartz-molybdenum association occur in the inner parts of the ore body as thin veinlets. The mineral association that is observed in the outer part of Medet porphyry system is quartz-pyrite-calcite, they occur as short veins. The ore mineralogy in the marginal and upper level of this deposit consist of quartz-galena-sphalerite, and they occur as short veins. The secondary enrichment of Medet porphyry system appear in the upper level. The oxidizing zone contain rare malachite, azurite, and cuprite. Meanwhile the secondary minerals consist of bornite, covellite, and chalcocite.

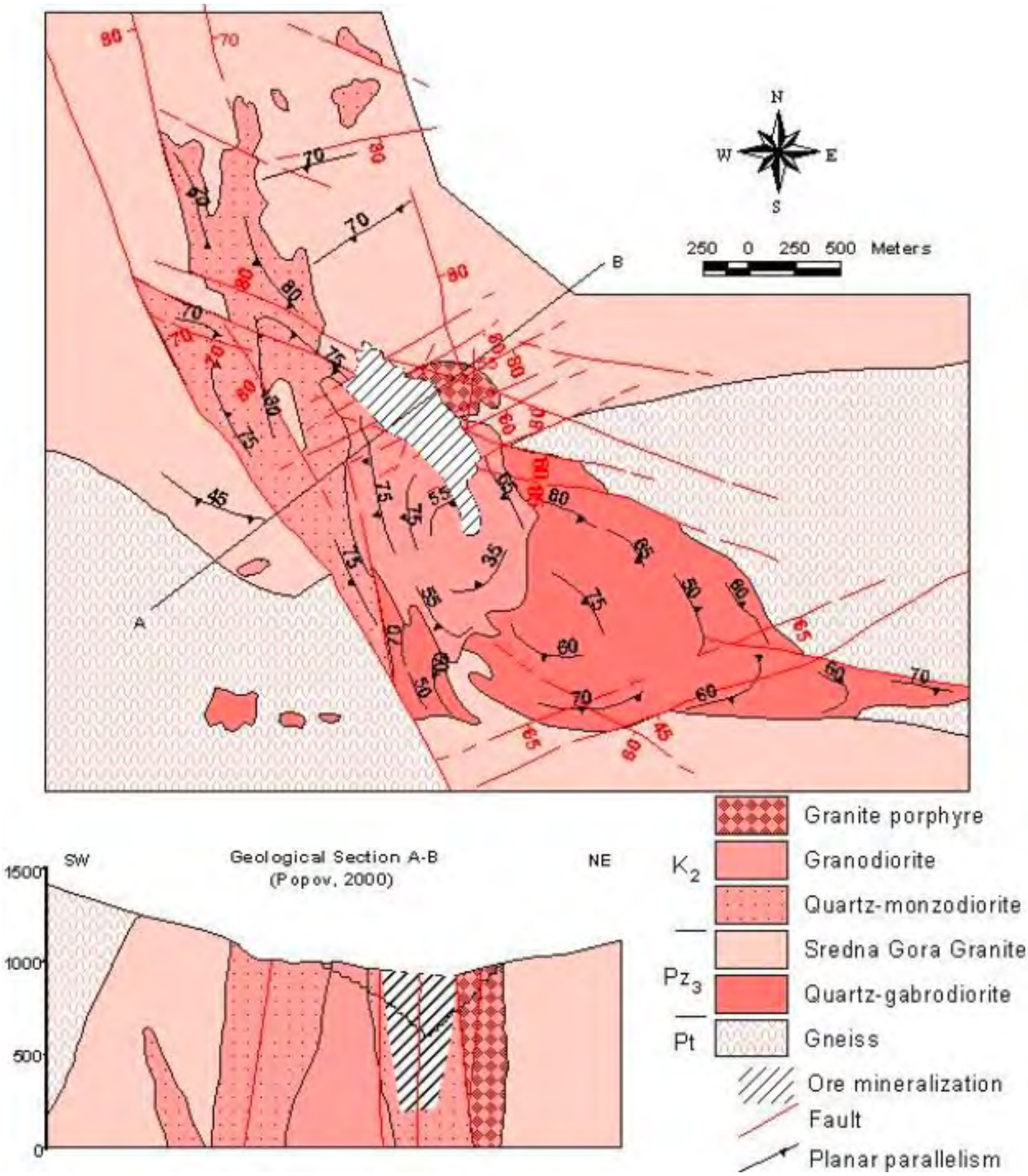

Figure 2: Map of the Medet porphyry copper deposit (from Strashimirov et al., 2003 after Popov and Bayraktarov, 1978).

Assarel Geology and Mineralization

The Assarel deposit is located ~6 km SE of Medet and associated with coeval volcanic. It is situated in the central part of the Assarel volcano with dense radial and concentric faulting and jointing (Figure 3). Nedialkov et al. (2006) divided the volcanic sequence into: (1) Hb andesites and latites; (2) Hb-Py to Px-Hb basaltic andeites; and (3) Bi-Hb andesite, Qz-andesites to dacites. This volcanic sequence was intruded by the Assarel porphyry intrusions in the center of the former stratovolcano

(Strashimirov et al., 2003). This intrusion is classified into: (1) Qz- diorite to Qz monzodiorite porphyris; (2) Qz monzodiorite to granodiorite porphyries; and (3) granite porphyry (Nedialkov et al., 2006). The published data by Lilov & Chipchakova (1999) reavealed time span from 91 to 81 Ma for the age of the main magmatic activity and the hydrothermal alteration. Meanwhile the U-Pb zircon dating by Peytcheva et al. (2007) revealed a narrow time span between 89.90 ± 0.26 Ma for the quartz diorite porphyry and 89.13 ± 0.28 Ma for a cross-cutting Hb-diorite porphyry dyke. Meanwhile Bi-Hb andesite of the volcanic succession is dated at 89.67 ± 0.78 Ma.

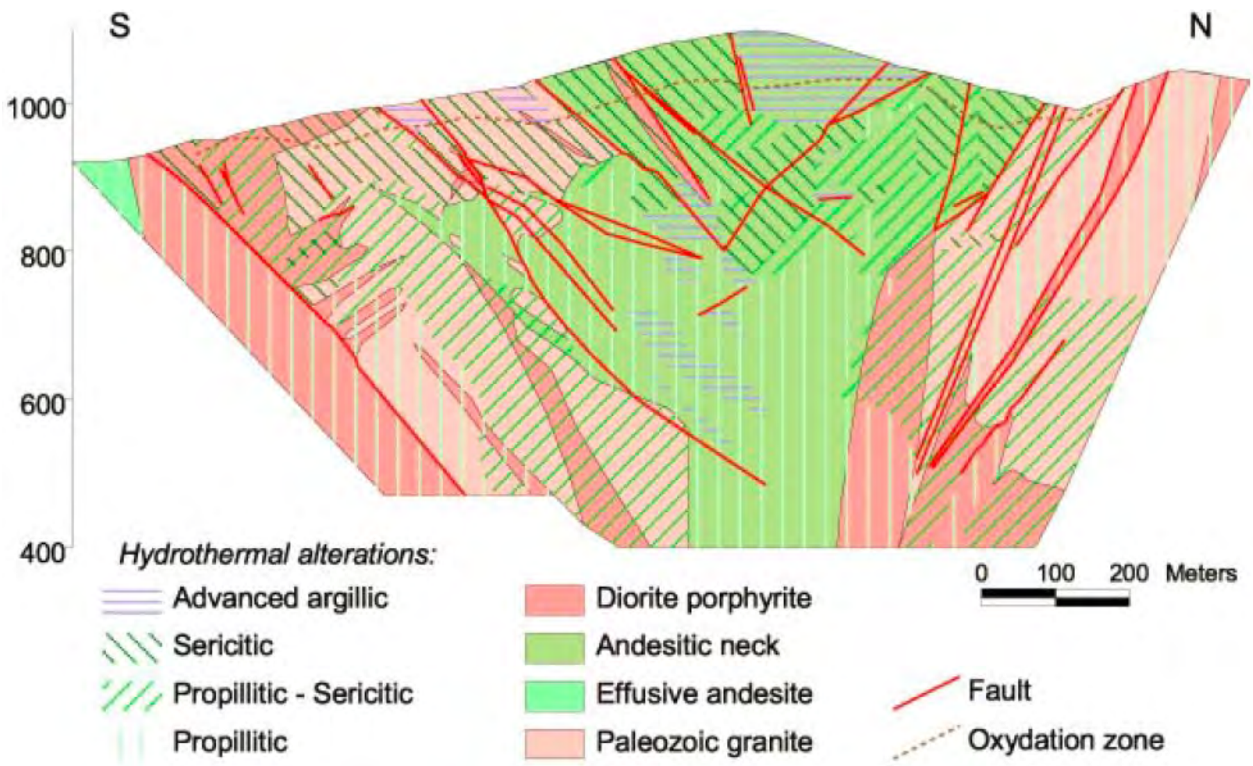

Figure 3: Stratigraphic section showing alteration types of the Assarel deposit (from Strashimirov et al., 2003 based on Popov et al., 1996).

The ore mineralization zone formed a cone-shape that is inclined by 80^o to 85^o in south or SW direction. The eastern part of the deposit is faulted that the altered basement of the metamorphic rock are now at the same structural level as the volcanic sequence (Strashimirov et al., 2003). Strashimirov et al. (2003) made a compilation of the alteration and the mineralogical composition of the Assarel porphyry system. The hydrothermal alteration of the Assarel porphyry system is composed of K-silicate, propylitic, and advance argillic. The advance argillic alteration has subtype of acid-chlorine and acid-sulphate. The propylitic and advance argillic alteration also sometime associated with the sericite alteration. The lithocap of the Assarel porphyry system is composed of sericitized epithermal alteration and advance argillic overprint over the propylitic and K-silicate alteration.
The ore mineral association compiled by Strahimirov et al., (2003) has similar

association with the one in Medet. The first ore mineral assemblage is quartz-magnetite-hematite±bornite±chalcopyrite, but the distribution is limited here. This assemblage also contain Ti-bearing minerals such as ilmenite. The main pervasive quartz-pyrite-chalcopyrite, occur as dissemination and veinlets in the middle and marginal part of the deposit. This assemblage in Assarel is associated with gold, Ni-Pd-As-, Cu-As (Te)-, Cu-Sn-V-, and Cu-Pb-Bi-bearing minerals. These association are found as inclusions in the chalcopyrite. The ore mineralogy in the upper level of this deposit consist of quartz-galena-sphalerite, and they occur as short veins. Galena and sphalerite are also found at depth in association with chalcopyrite veins. The secondary enrichment of Medet porphyry system appears in the upper level, overlies the primary quartz-pyrite-chalcopyrite mineralization zone. Near the contact of the oxidizing zone and the secondary enrichment contain high geochemical anomaly of Au (Strashimirov, 1993). The lithocap of Assarel porphyry consist of 60-70 m thick of supergene blanket mineralization of chalcocite and covellite.

Secondary Enrichment Proccess

Both deposits can be classified as epithermal to mesothermal epigenetic, structurally controlled, formed by replacement and open-space filling processes.

Secondary enrichment process is illustrated by the fluid path 1 on figure 4 (Sillitoe 2005). The process occurs in three steps. First step is the oxidative weathering: under the influence of aqueous fluids of the surface origin metal cations and SO_4^{2-} anions are leached from the zone above the water table. After that, the cations, for instance Cu2+, are transported down in solution Third step is the precipitation under reduced conditions with participation of HS^- - which leads to formation of minerals richer in Cu. Sulphide oxidation is catalyzed by bacteria: they assist reactions as Fe^{2+} to Fe^{3+} and S to SO_4^{2-}. The general reaction of precipitation of cations from solution in the presence of HS^- is as follows:

$Cu^{2+} + HS^- = CuS + H^+$

The resulting textures reflect the mass transport that accompanies the leaching process, which is reflected in fragmental textures, presence of pores and increased permeability of the rocks.

Path 2 on figure 4 shows the process of oxidation of chalcocite minerals to tenorite in the presence of pyrite.

$0.4{*}Cu_2S + O_2 = 0.4\ CuO + 0.4\ CuSO_4$

In order to allow the transport of Cu, pH of at lower than 5.5 is required. Therefore, low acidity and low pyrite content result in little transport of Cu. Precipitation of Cu in the saturated zone below the water table happens by exchange of Cu to Fe and other metals with lower electronegativity from hypogene sulfide minerals. Replaced Fe goes into limonite, while Zn and Pb are disseminated and only rare cases of Zn and Pb enrichment are reported.

The following most important factors control oxidation and enrichment processes:

Orebody geometry	Source rock of Cu for secondary enrichment should be thick enough to generate the enrichment zone	Vertically extended breccia pipes – ideal geometry
Structural features	Faults are responsible for permeability necessary for transport of fluids	Steep, throughout going faults are favourable
Mineralogy of sulfides	Pyrite is important for generating acid solutions that mobilize Fe and Cu	Optimal ratios of Pyrite to chalcopyrite of 4:1 to 5:1 (higher ratios – deficiency of Cu)
Alteration assemblage	Acid-buffering capacity and permeability	Potassic, sericitic, advanced argillic alteration

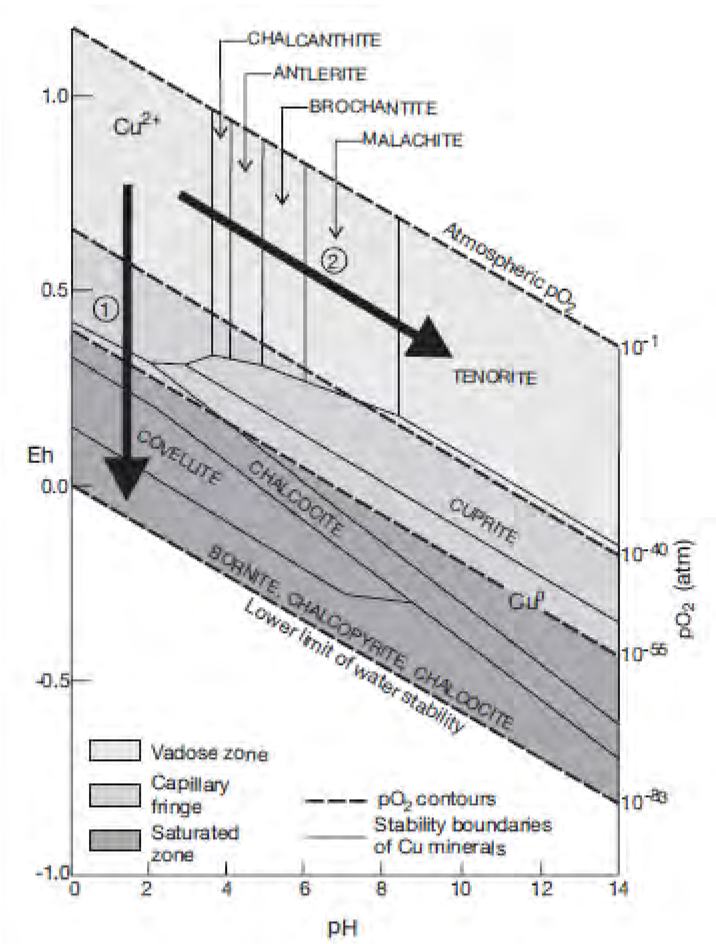

Figure 4: Phase diagram of common supergene Cu sulphides in the Cu-S-H system, from Sillitoe (2005).

The following fluid inclusion homogehization temperatures were obtained for the fluid inclusions from Medet and Assarel deposits:

Mineral association	Medet	Assarel
Q-KFsp	>500	
Q-Mt-Hematite	400-380	
Q-Py-Chpy	390-320	310-290
Q-Mo	330-300	

Q-Py	310-280	230-215
Q-Ga-Sph	280-240	195-150

In the initial stages of formation of Medet deposit, the participation of meteoric waters was limited. In contrast, Assarel is characterized by more intense reworking of the host rock, shallower level, more intense alteration and was more open to meteoric waters.

References:

Peytcheva, I., von Quadt, A., Heinrich, C. A., Nedialkov, R., Neubauer, F., & Moritz, R. (2007, August). Medet and Assarel Cu-porphyry deposits in Central Srednogorie; SE Europe: were they a common magmatic and hydrothermal system. In *Proceedings of the Ninth Biennial SGA Meeting, Dublin* (Vol. 2, pp. 881-884).

Sillitoe, R. H. (2005). Supergene oxidized and enriched porphyry copper and related deposits. *Economic Geology One Hundredth Anniversary Volume (Heddenquist, JW; Thompson, JFH; Goldfarb, RJ*, 723-768.

Strashimirov, S., Bogdanov, K., Popov, K, & Kehayov, R. (2003). Porphyry systems of the Panagyurishte ore region. *Cretaceous porphyry–epithermal systems of the Srednogorie zone, Bulgaria. SEG Guidebook Series*, *36*, 47-78.

Magma, Mixing and Mingling (Vetren Boshuyla)

Process and conditions of magma mixing and mingling in a magma chamber is a fascinating topic. These mechanisms are mostly known as commingling of magmas of different compositions (Sparks and Marshall, 1986).

Mixing and Mingling in a magma chamber – process and conditions

Based on field observations by Wiebe et al. (2002), hotter mafic materials intrude as dike into a cooler silicic magma chamber. During this process, the different magmas can be mingled or mixed together. While in the first process no chemical exchange between the magmas occur, a wide range of replacement is possible in the second one, strongly depending on the heat transfer among them. The spectrum reaches from a partial exchange to the formation of a new hybrid melt. For this hybridization, Wiebe et al. (2002) are discussing four possible settings.

1) Prior to emplacement: after comparing petrographic relationships and compositions of mafic dikes and margins of mafic layers, hybridization is an unimportant process.
2) During emplacement into the chamber: the rise as dike into a solid granite and a crystal poor interior provides a dynamic environment for hybridization. Commingling was observed over several meters in the only feeder dike at the research location. Flow front instabilities and further movements led to separation of the mafic material, which may have caused the detected structures, e.g. mafic lenses in granites.
3) Interactions along the base of the mafic sheet: the flowing mafic magma is instable and starts to break (Snyder and Tait, 1995). Due to a lower density, small portions of silicic magma start to percolate upwards. Some of the silicic magma will possibly mix with the mafic material. (Figure 1)
4) Interactions along the top of the mafic sheet: it is important that the upper granitic layer has a higher density than the lower mafic. Under these conditions, the cooler overlying layer can mix with the one below, leading to zones with larger crystals from the granite and fine-grained mafic material. (Figure 1)

Requirements for the process of magma mixing and mingling are two different magmas, usually a more silicic and more mafic magma is involved. After Wiebe et al. (2002) and Bain et al. (2013), the hotter mafic magma injects into a magma chamber containing a silicic magma or silicic crystal mush layers, respectively. The silicic magma is usually more viscous and colder, in comparison to the mafic magma. The temperature difference, in addition with the varying viscosity can lead to instability in the flow front of the mafic magma. This leads to a phenomenon in the form of blunt fingers (Snyder & Tait, 1995). With ongoing movement, the effect is boosted and can lead to separate mafic magma lenses in the silicic one (Figure 2). Also different shapes of mixing/mingling, such as flame structure or granitic pipes into mafic magmas are possible. If one or another structure is formed, depends on the thermal rheological contrasts as well as on the relative proportions between the magmas (Wiebe et al., 2002). As seen before, the heat transfer between the magmas is an important aspect for mixing between them. This can lead to crystallization and therefore associated changes in physical properties of the magmas as they mix (Sparks and Marshall, 1986). But as long as there is no relevant heat transfer between the magmas, they can mix together physically but compositional heterogeneities are still preserved in the rocks. After Sparks and Marshall (1986) is this process named with the term commingled magmas.

The plutons of the Upper Cretaceous South Srednogorie Zone, Bulgaria

In the southern part of Central Srednogorie a chain of plutons intruded (e.g. Boshulya, Velichkovo, Vurshilo) in the Pre-Upper Cretaceous basement along a large-scale dextral strike-slip fault, the Iskar-Yavoritsa shear zone, and some minor shear zones parallel and oblique to it. Magma emplacement occurred in laccolith-like chambers and the plutons show characteristics of layered intrusions, i.e. the sequences of deposits are record of magma chamber processes that were active during crystallization. (Figure 3) (Peytcheva et al., 2008)

The lower part of the plutons consists of gabbro diorite porphyries, diorites and granodiorites. The upper parts are composed of granites. The part in-between those two is a mingled/mixed level of thin sheet-like gabbro and intruded gabbro-diorite bodies. Load casts and chilled zones as well as flame structures and veins of leucogranite characterize the bottoms of these mafic sheets. The top of the mafic sheet is composed of swarms of basic to intermediate enclaves. Most mafic sheets are sub horizontal and highly elongated, swarms of enclaves are parallel to it. Mafic feeder dykes crosscut the intermediate layer between the gabbroic and the granitic part. These relationships provide evidence for long-living magma chamber with magma replenishment. (Figure 4 and 5) (Peytcheva et al., 2008)

Both the gabbros and diorites show signs of magma mixing and have similar mineral composition: plagioclase, hornblende, clinopyroxene, k-feldspar and quartz. The felsic rocks consists of plagioclase, k-feldspar, quartz, biotite and rarely hornblende. Common accessory minerals in all rocks are apatite, zircon and magnetite ± titanite. Anderson and Smith (1995) derived P-T-conditions of magma crystallization from hornblende thermometry and geothermobarometry. They range for the hybrid gabbroic rocks from 900-700 °C/7.0-6.5 kbar (cores) and to 680 °C/2.5-1.8 kbar (rims), which gives two possible levels of crystallization of plagioclase and hornblende in 15-18 km and 4-9 km depths. (Peytcheva et al., 2008)

Major and trace element analysis of samples from the different plutons suggest a complex evolution of the magma. The strong negative Nb anomaly as well as REE patterns is typical for subduction related magmatic succession. Negative Eu anomaly was not observed, thus plagioclase was not fractionated from any of the magma

suites. Further trace-element analysis shows an enrichment of Th, Ba and Sr, suggesting the initial magma was produced by slab derived fluid and minor sediment derived. These data suggest the metasomatized mantel wedge as the primary magma source. (Peytcheva et al., 2008)
Calculated ages for zircons in the Elshitsa-Boshulya and Vurshilo plutons are around 86.5-86 (Elshitsa granite), 85-84.5 (Velichkovo granodiorite, Velichkovo hybrid gabbro) and 82 Ma (Vurshilo granite; Velichkovo hybrid gabbro). These results indicate events in at least two magma chambers (region around Elshitsa in the North, and Bolshulya, Velichkovo and Vurshilo in the South) at a certain time. The field structures (load casts, flame structures, globular enclaves) of the 82 Ma event indicate interaction of the gabbroic magma with not fully solidified, but colder granitic mush. (Peytcheva et al., 2008)
Saturation of zircon is mainly sensitive to temperature and zirconium concentration of the magma, minor to whole-rock chemistry and H_2O-content. Zirconium is an incompatible element and therefore its concentration in the primary magma is usually low and the high temperature of magma will not allow zircon saturation. Zircon is expected to crystallize after a drastic change in temperature or in zirconium concentration. Mingling and mixing processes with colder granitoid magma/mush in the middle-upper crustal chambers favor fast cooling of gabbroic magma and magma degassing. Both processes lead to zircon saturation, which explains the present of zircons in the hybrid gabbros. This new zircon saturation is important for dating the mingling/mixing process of the South Srednogorie plutons. (Peytcheva et al., 2008)
The Sr and Nd characteristics and trace-element signature of the basic hybrid rocks remains primitive. This suggests that mingling/mixing of the gabbroic magma with the felsic magma occurred with fractionally crystallized magma with little crustal contamination. (Peytcheva et al., 2008)
In the Upper Cretaceous South Srednogorie Zone, the special case of crystallization of zircons together with rock-forming minerals in shallow magma chambers occurred due to mingling/mixing of hybrid gabbroic magma. (Peytcheva et al., 2008)

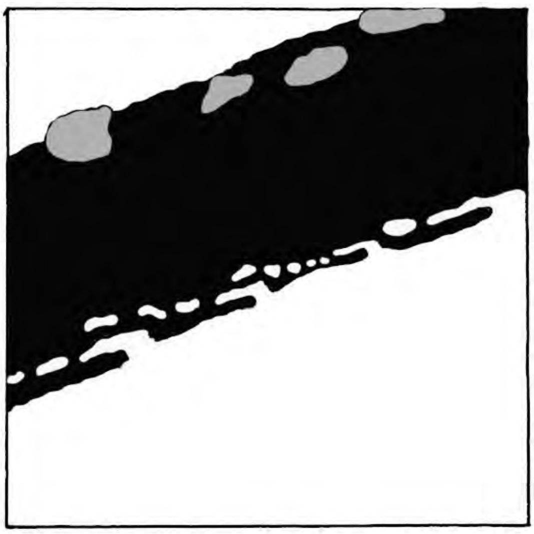

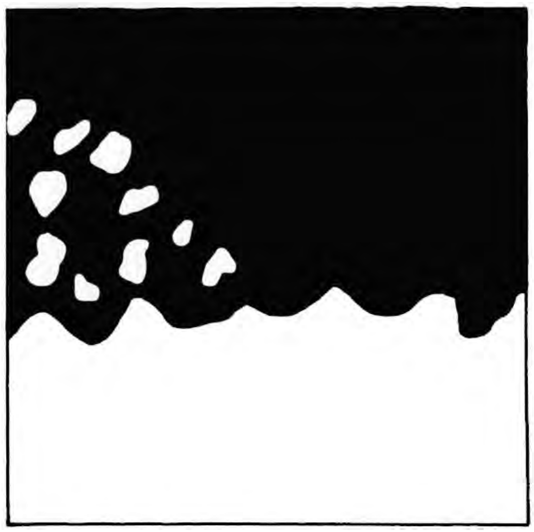

Figure 1: Interactions of silicic magma along the base (blunt finger structures and magma lenses) and the top (gray: mixing between the different magmas) of the mafic sheet. Modified after Wiebe et al., 2002.

Figure 2: Possible structure resulting from mingling/mixing processes.

Modified after Wiebe et al., 2002.

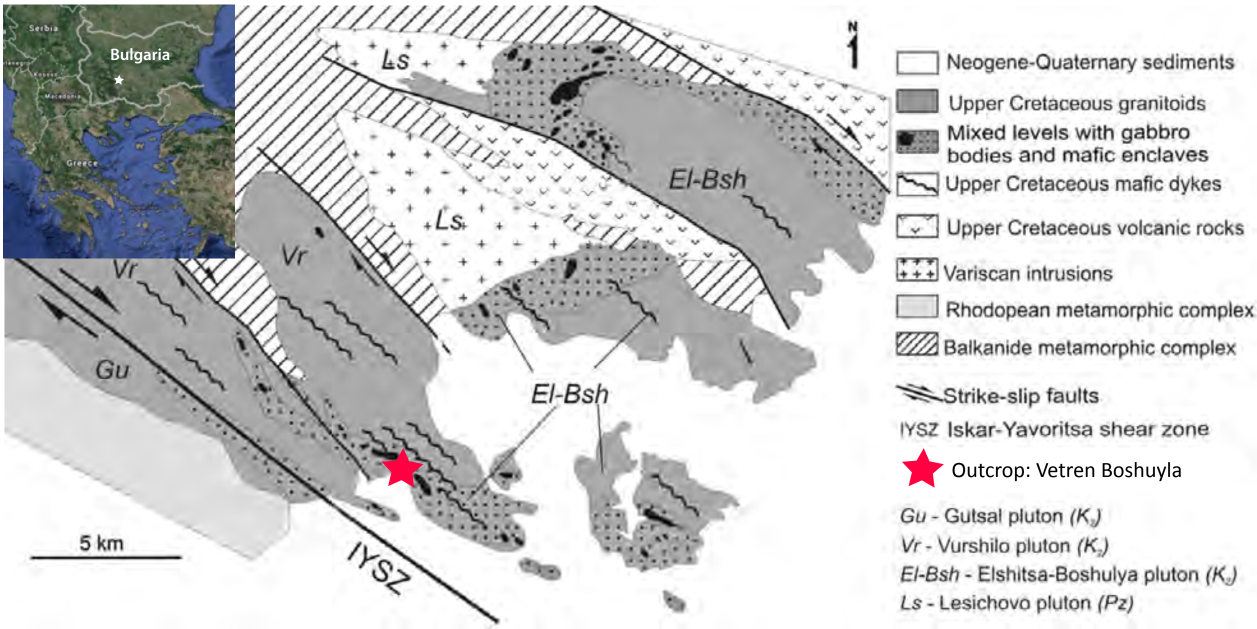

Figure 3: Map of the Balkan Peninsula (colored, modified after googlemaps) with the star at the position of the geological map of the area where the plutons Vurshilo, Elshitsa-Boshulya and Velichkovo appear at the surface along the IYSZ. Modified after Peytcheva et al., 2008.

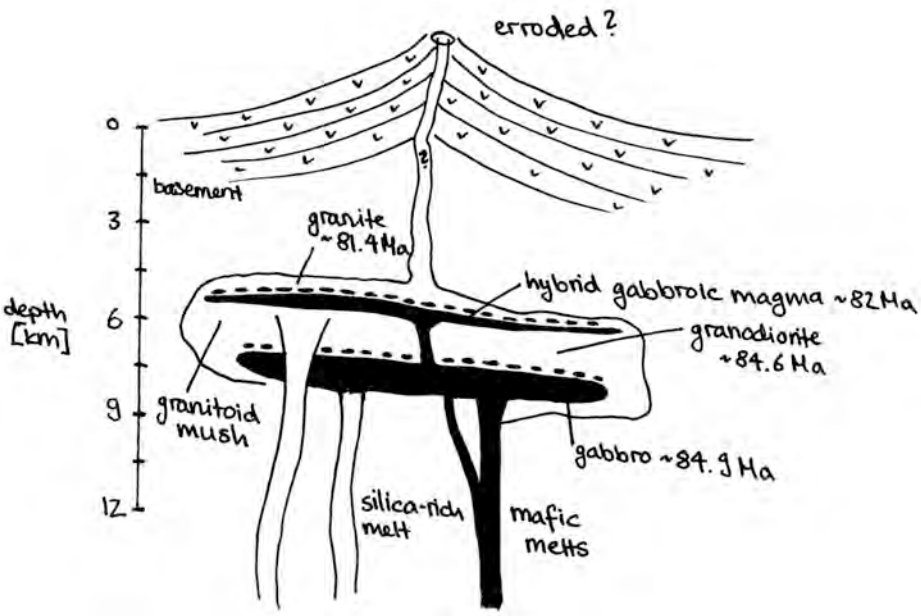

Figure 4: Mafic enclaves in granitic rock, load casts in upper mafic layer and evidence for compaction at the upper boundary of the lower layer. Feeder is dioritic in composition. (Wiebe et al., 2002)

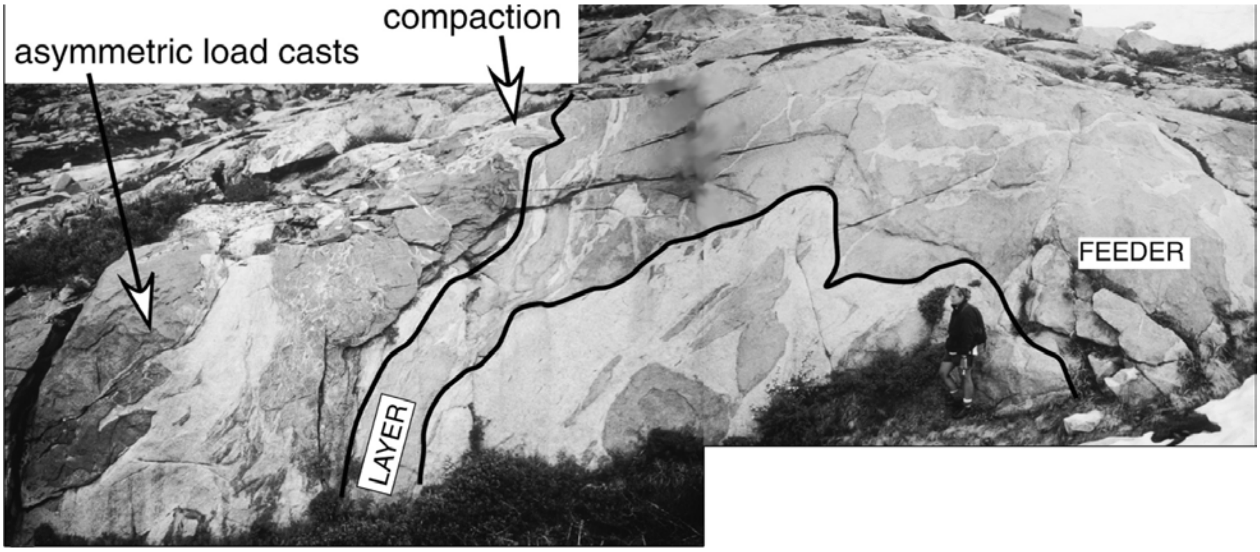

Figure 5: Schematic sketch of the evolution of the magma chamber producing Boshulya, Velichkovo and Vurshilo plutons.

1. Basic magma intrudes a stratified chamber at 84 Ma, almost simultaneously with a granodiorite. Mafic enclaves are formed above the sheet-like hybrid gabbroic body.
2. a second gabbroic magma enters the chamber using conduit dikes at 82 Ma. Hot basaltic magma mixes with the granitoid mush.
Hot deep crustal zones with hydrous basaltic magma generate intermediate and silicic igneous rocks through fractional crystallization and partial melting of pre-existing crustal rocks.
3. Vurshilo granite forms above the sheet-like body of the hybrid gabbro.
Modified after Peytcheva et al., 2008.

References

Anderson, J.L., Smith, D.R., 1995. The effects of temperature and fO2 on the Al-in-hornblende barometer. American Mineralogist 80, 549-559.

Bain, A.A., Jellinek, A.M. and Wiebe. R.A., 2013. Quantitative field constraints on the dynamics of silicic magma chamber rejuvenation and overturn. Contrib Mineral Petrol, 165:1275-1294.

Peytcheva, I., von Quadt, A., Georgiev, N., Ivanov, Zh., Heinrich, C.A. and Frank, M., 2008. Combining trace-element compositions, U-Pb geochronology and Hf isotopes in zircons to unravel complex calcalkaline magma chambers in the Upper Cretaceous Srednogorie zone (Bulgaria). Lithos 104:405-427.

Snyder, D. and Tait, S., 1995. Replenishment of magma chambers: Comparison of fluid-mechanic experiments with filed relations. Contrib Mineral Petrol, 122:230-240.

Sparks, R.S.J. and Marshall, L.A., 1986. Thermal and mechanical constraints on mixing between mafic and silicic magmas. J Volcanol Geotherm Res, 29(1-4):99-124.

Wiebe, R.A., Blair, K.D., Hawkins, D.P. and Sabine, S.P., 2002. Mafic injections, in situ hybridization, and crystal accumulation in the Pyramid Peak granite, California. Bull Geol Soc Am. 114(7):909-920.

The geology of the Rhodope Massif

Introduction

This brief geological overview of the Rhodope Massif is based on the research of (Burchfiel et al., 2008), (Burg, 2012), (Hinsbergen and Schmid, 2012) and (Marchev et al., 2015). The Rhodope Massif is a high-grade metamorphic duplex system located in Southern Bulgaria. The massif is a deformed segment of the Alpine-Himalayan suture and collision system and makes up a 300 by 300 km open antiformal structure. The northern side of the massif is bounded by the Maritza fault, the southern side by the Strymon detachment. Collision between the African and Eurasian plate resulted in a northeast dipping subduction zone. The rocks were partly subducted to UHP metamorphic conditions and retrogressed to amphibolite facies during Cretaceous times. Associated crustal thickening resulted in syn-

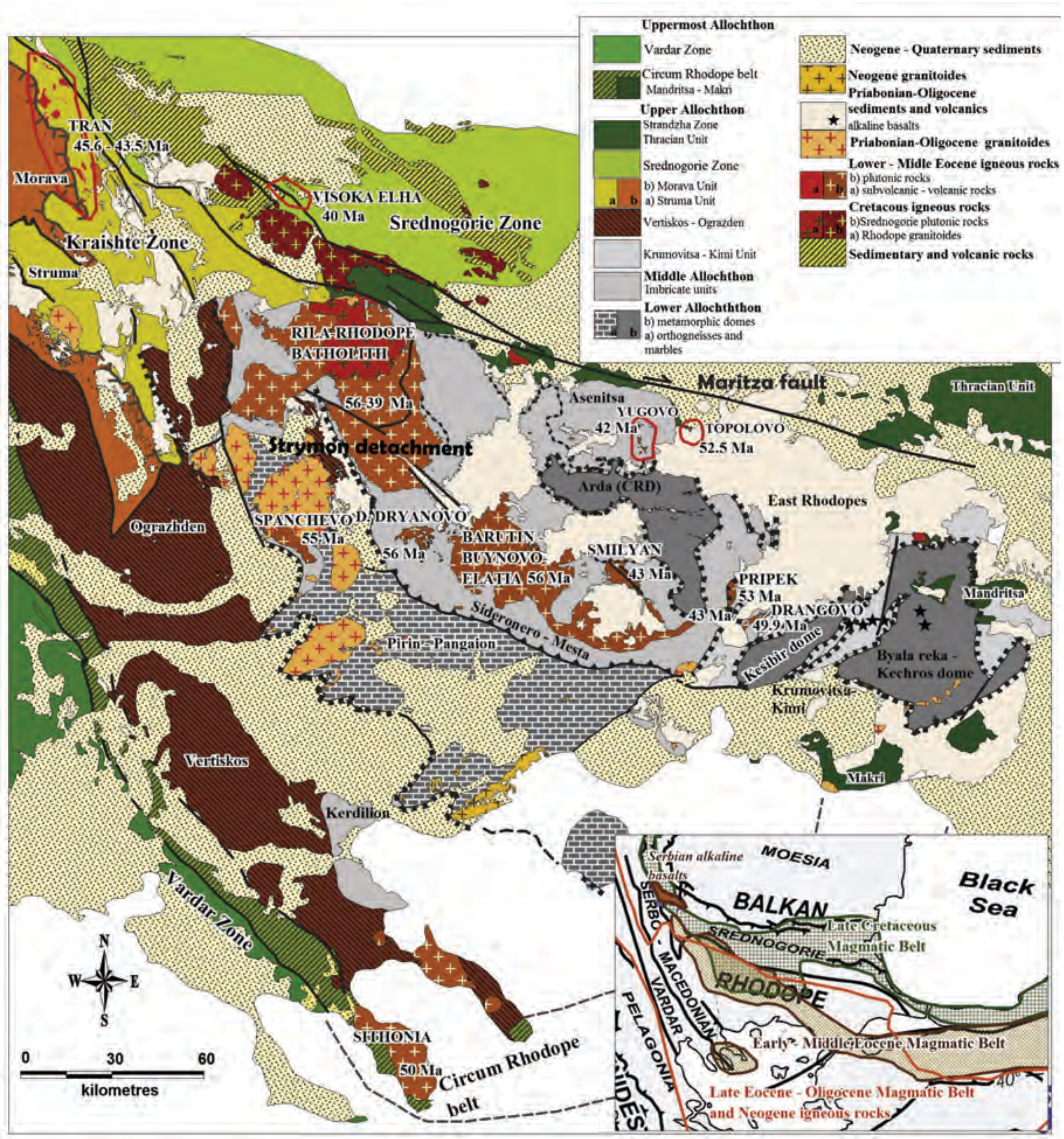

Figure 7: Geological overview of the Rhodope Massif modified after Marchev et al., 2015. Maritza fault and Strymon detachment are indicated, as well as the Smilyan granite intrusion. The small picture (lower right corner) shows the relative position of the Rhodope massif to the Moesia platform and Black Sea.

orogenic extension and exhumation. Consequently a nappe stack was formed, with the highest grade metamorphism (UHP rocks) units thrusted on top of lower grade units. This nappe stack is namely consisting of mylonitic gneisses and is tansgressively overlain by deep to-shallow low water sediments (48-42 Ma) and intruded by Tertiary granitoids. Deformation took place during Cretaceous and early Paleogene time, and magmatic activity is associated with Early-Middle Eocene and Oligocene.

Present-day crustal structure of the Rhodope Massif

During the late Jurassic the subducting Tethys plate (African plate) below the European plate represented a 'classic' subductional setting. This included dehydration melting, which led to rising magmas and ultra-high pressure rocks, forming the continental magmatic 'Rhodope' arc. Ongoing subduction of the continental passive margin dragged this forearc lithosphere into subduction. The arc system reached its deepest subduction during 130-115 Ma. This was followed by the fast upward return of the Rhodope arc to the amphibolite facies, coeval with crustal stretching (110 Ma) and slab roll-back. A combination of rock uplift, extension, mantle delamination and slab retreat during the Eocene-Oligocene separated the mantle from the crust as it opened. Hot asthenosphere flowed into the gap and led to partial melting and magma generation (Figure 2). The magma could intrude into the upper crust and formed post-orogenic plutons. The hot asthenosphere replaced the heaviest asthenosphere and triggered isostatic uplift, creating new topography. This subduction-exhumation cycle resulted in the crustal structure of the Rhodope massif, indicated by the Maritza fault and the Strymon detachment bounding the metamorphic "Rhodope" dome-complex and the presence of several granite intrusions (e.g. Smilian granite, see figure 1).

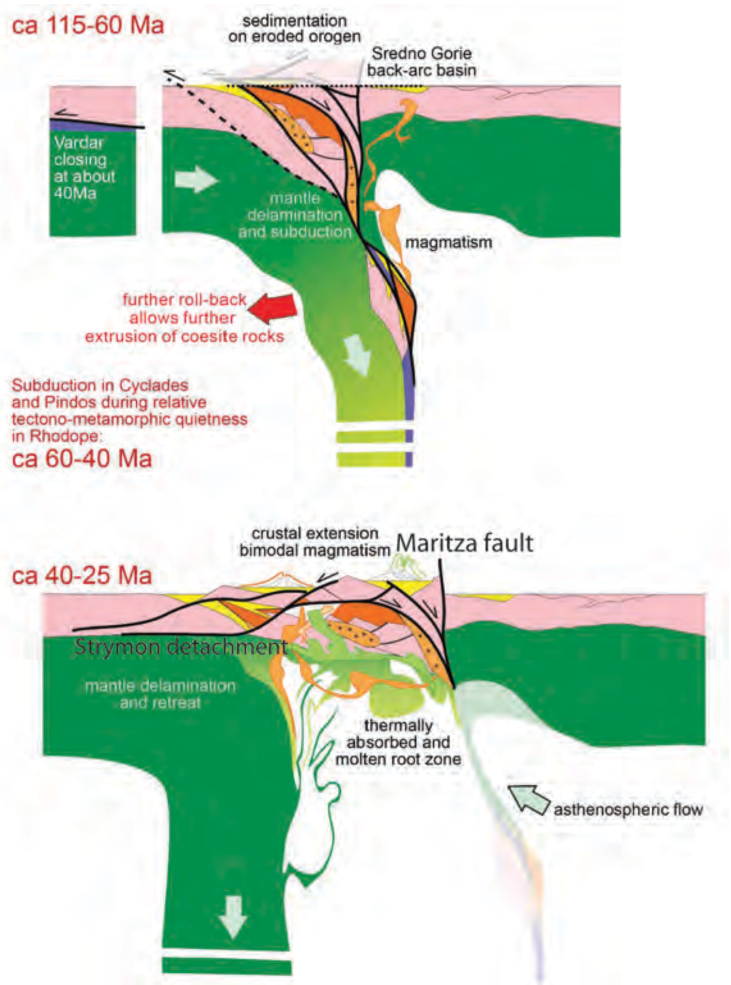

Figure 8: Tectonic interpretation of Rhodope island arc in Late Cretaceous and Oligocene times modified after Burg, 2012. Upper picture: slab rollback led to exhumation. Lower picture: mantle flows into gap formed by separation of mantle from crust, leading to uplift and creation of present structure and topography.

Tectonism

Transition from regional compressional to extensional system
The triangle shaped metamorphic Rhodope massif is part of the Southern Balkan extensional system, situated north of the North Anatolian fault. Extension in this area began in the Paleogene or latest Cretaceous during the final closure of the Vadar Ocean and took place in a larger regional convergent setting created by the evolving subduction system. The tectonic setting during deformation of the Southern Balkan extensional system can be divided into four stages:

1. Late Cretaceous to Paleogene extension within a regional compressional system.
2. Middle Eocene to late Oligocene extension associated with abundant volcanism.
3. A short period of local shortening.
4. Middle Miocene to present regional extension.

The transition from a regional compressional to a regional extensional setting took place in the Paleogene, between stages 1 and 2. This transition is associated with the termination of subduction of the Vadar ocean. During the late Miocene the North Anatolian fault formed, decoupling the deformation in the Aegean from the Southern Balkan extensional system.
Due to crustal thickening in the late Cretaceous and Paleogene metamorphism into the eclogite and amphibolite facies and volcanism took place. Furthermore, numerous low angle shear zones and faults generated at time of high-grade metamorphism are visible as relicts in the Rhodope massif.
Contemporaneous compression and extension
The thickened crust of the Rhodope mountains was relatively hot, which is indicated by abundant magmatism and the metamorphic conditions of the rocks. This hot crust could spread laterally, driven by gravitational potential energy. Moreover, this lateral spreading could be accommodated by thrusting at deeper crustal levels and by contemporaneous extension at shallower crustal levels, generated by faults. These faults could be found as detachment faults in regional extensional environments. Unfortunately, such detachments are not found in the Rhodope area. Furthermore, regional extension is associated with crustal thinning and basin development. During early extension, which formed under a regional compressional system (stage 1) the formation of such basins is lacking. During the later regional extensional system (stage 4) basins were formed. This shows nicely the difference in features of the Paleogene and the Neogene, indicating the change in the tectonic environment.
Exhumation of the Rhodope massif
An important extensional detachment in the Rhodope massif is the top-to-the-southwest Strymon detachment, which is active since the Miocene. Exhumation of the Rhodope massif took place by a system of extensional unroofing. The extensional history of the Rhodope seems to have developed in two stages. In the first stage, since the early Eocene, extension affected the area from the Mesta Graben in the northwest to the Thrace basin in the east. With the largest extension in the central part of the Rhodope (about 15 km) and decreasing extension towards the poles of rotation. Extension in this stage was accommodated by opposite rotations of the poles of about 2°. In this stage only a small lense-shaped basin opened. In a second stage between 25-5 Ma, major extension occurred along the Strymon fault

and was associated with a 25° clockwise rotation of the NW pole at the Mesta graben. This stage resulted in the opening of the Mesta graben, Thrace basin and in the exhumation of the Rhodope massif with its triangle shaped form.

Magmatism

The Rhodope Massif Complex (RMC) is partially composed of plutons and subvolcanic rocks. The plutons consists of equigranular to porphyric granodiorites, biotite-rich granites and tonalities. They are represented either as individual plutons or as phases in composite plutons or batholiths.

From geochronological methods, the age of the plutons has been assigned to 56 to 42 Ma (Early to Middle Eocene). Magmatic rocks of the similar ages can be traced for 250 km from Eastern Serbia to the RMC in South Bulgaria, and is referred to as the Early-Middle Eocene Magmatic Belt. The magmatic event is even visible over 1000 km to Northern Turkey (as calc-alkaline and intrusive rocks). This indicates a large-scale post-collisional tectonic process.

The plutons of the RMC are predominately adakitic in composition – that is, a magmatic signature of intermediate to silicic composition. It is characterized by a high silica content (60 - 76 wt.%), elevated Al_2O_3 (>15 wt.%), MgO (>3 wt.%) and depletion of HREE and Y. Accessory minerals are abundant (especially in the older plutons), and found as apatite, zircon and magmatic epidote.

The origin of the adakitic plutons has been debated. As mentioned, the magmatic event was caused by a large-scale post-collisional tectonic process. The depth of emplacement for the RMC plutons was at ~15-16 km – determined from Al-in-hornblende barometry and the occurrence of primary epidote.

The precursor for the adakitic rock is believed to be basaltic (from mafic enclaves in granodioritic plutons), and originated from the mantle. They were metasomatized (chemically altered due to interaction with fluids) during subduction processes. This is a result of the closure of the Northern Neotethys Ocean. An early fractionation of amphibolite, biotite, magnetite and epidote increased the silica-content, and fractional crystallization in the lower/middle crust was crucial for the evolution of the adakitic rocks.

As a conclusion most of the volcanism is associated with an extensional event starting in the Paleogene (stage 2, see tectonic section). Asthenospheric upwelling and orogenic collapse caused heating and fast exhumation of the Rhodope metamorphic basement in the interval 42-35 Ma and formation of core complexes. After 35 Ma, the magmatism transitioned to a normal, extensional calc-alkaline event in Late Eocene – Lower Early Oligocene. Magmatic activity ceased by the end of Oligocene.

References:

Burchfiel, B. C., et al. "Evolution and dynamics of the Cenozoic tectonics of the South Balkan extensional system." *Geosphere* 4.6 (2008): 919-938.

Burg, J.-P., 2012. Rhodope: from Mesozoic convergence to Cenozoic extension. Review of petro-structural data in the geochronological frame. In: Skourtos, E., Lister, G.S. (Eds.), The Geology of Greece, Journal of the Virtual Explorer. 42 Paper 1, 42 Paper 1

Hinsbergen, Douwe JJ, and Stefan M. Schmid. "Map view restoration of Aegean–West Anatolian accretion and extension since the Eocene." *Tectonics*31.5 (2012).

Marchev, P. et al. Adakitic magmatism in post-collisional setting: An example from the Early-Middle Eocene Magmatic Belt in Southern Bulgaria and Northern Greece, Lithos (2013), http://dx.doi.org/10.1016/j.lithos.2013.08.024.

Overview of hand drawn pictures

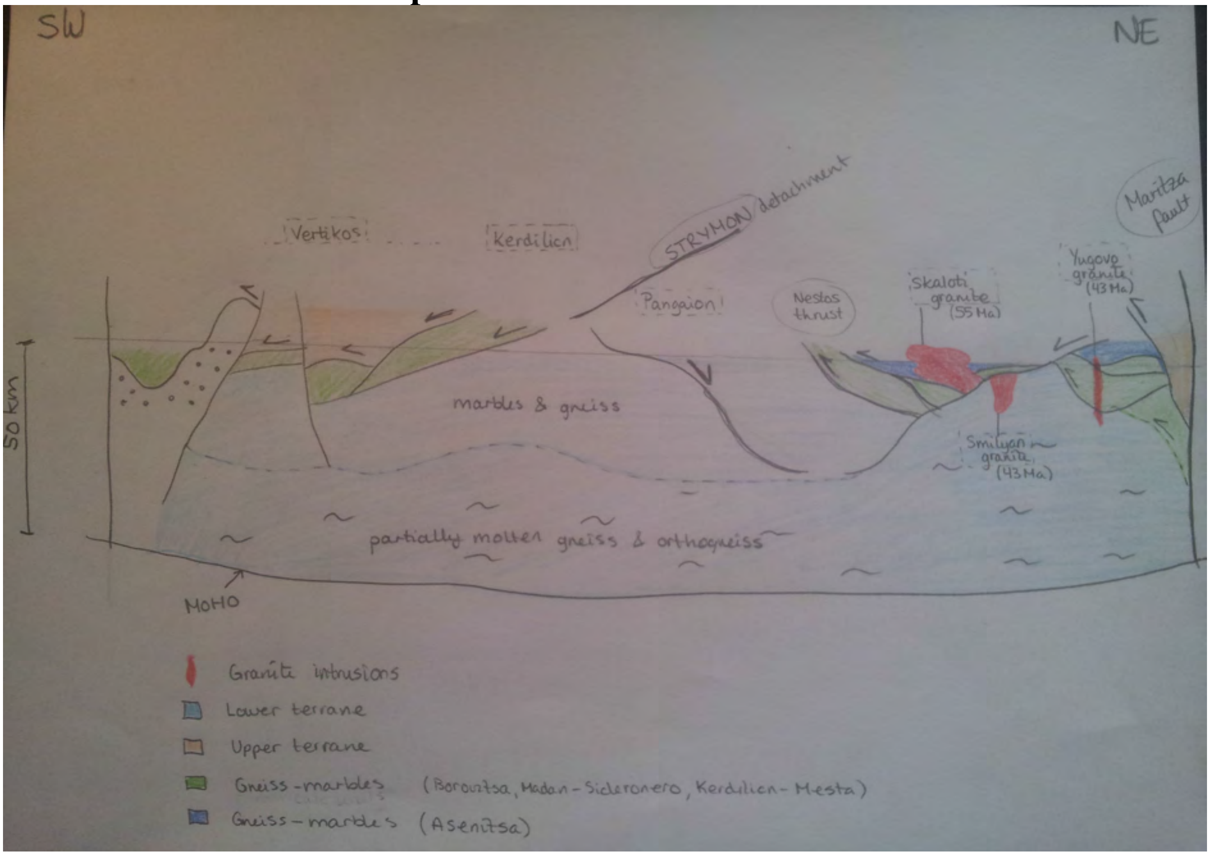

Profile of the Rhodope massif after Burg 2012, with the intrusive granitoids, the Strymon detachment, the Martiza fault and Nestos thrust indicated. Movement direction is shown by arrows.

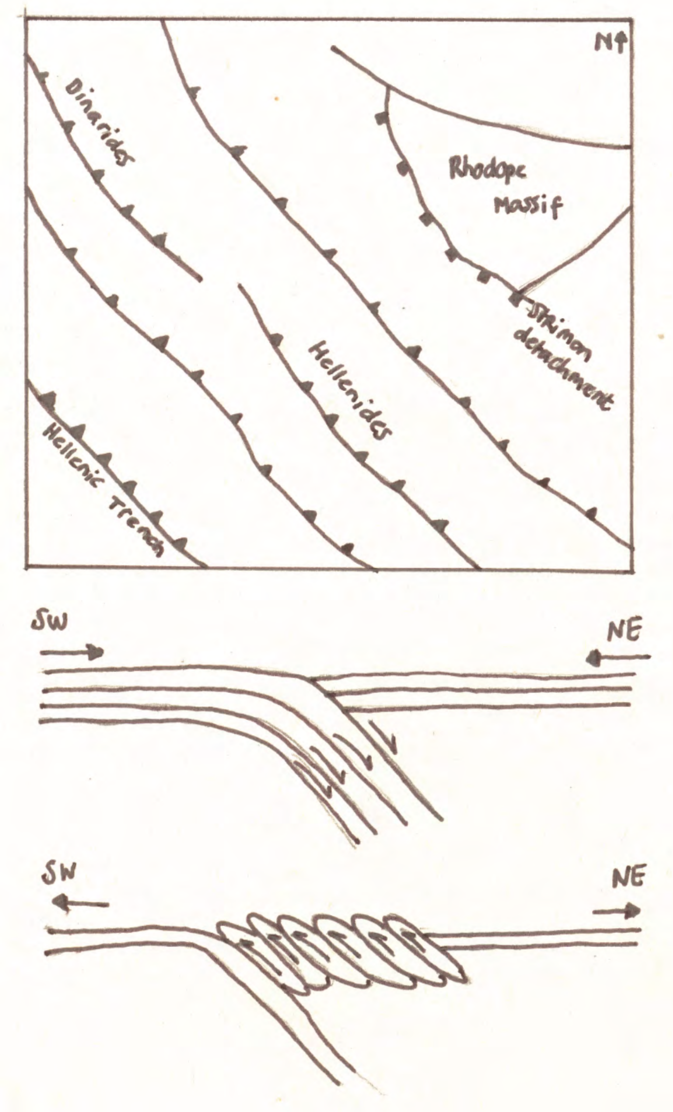

Schematic and non-scaled overview of formation of nappe stack.

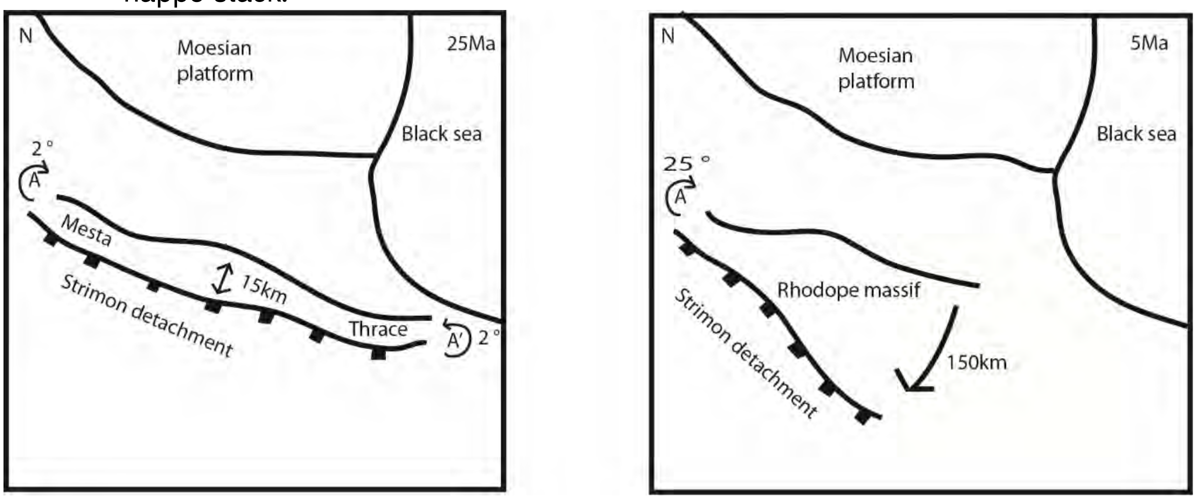

Evolution of the Rhodope massif after Hinsbergen and Schmid, 2012. Left: small lense shaped basin is formed by small opposite rotation around pole A and pole A'. Right: Larger clockwise rotation around pole A leads to opening of Mesta and Thrace basin and

Pb-Zn deposit Madan, Laki

The Central Rhodope dome (Rhodope Massif, Southern Bulgaria and Northern Greece) hosts several important Pb-Zn ore fields, including Madan, Eniovche, Laki, and Davidkovo in Bulgaria (Fig. 1). All of these vein and replacement deposits occur close to the detachment fault. About 9 Mt of zinc and lead metal were mined or are still present in at least 70 individual deposits, to which the Madan ore field contributes 78%. The richest and largest orebodies were formed by hydrothermal replacement of marbles, but significant resources were mined from veins. Presently, three underground mines are active (Laki-Djurkovo, Madan-Krushev Dol, and Eniovche), with an average production grade of 2.90% Pb and 2.16% Zn at Laki and 2.54% Pb and 2.10% Zn at Madan (Rohrmeier et al, 2013 and references therein).

1. Geology background

The Central Rhodope Dome (**CRD**) consists of high grade metamorphic rocks including granitic gneisses, amphibolites, mica-schists and marbles. The dome is bound by extensional detachment faults and shares many characteristics of metamorphic core complexes e.g. (Ivanov, 1988; Burg et al., 1990; Ivanov et al., 2000). It can be separated into a number of different tectonic units (Fig. 1). The footwall part of the Dome consists of **the Arda unit** (high-grade metamorphites affected by intensive migmatization and anatexis) and **the Madan unit** (migmatite orthogneisses, amphibolites, mica-schists and some marble packages). The hanging wall is represented by **the Asenitsa unit** (marbles, amphibolites and orthogneisses) and by **undeformed Paleogene Sediments** (argillites, breccias, conglomerates, sandstones and marly limestones) (Ivanov et al., 2000). Units are separated by synmetamorphic shear zones, corresponding to either reactivated early Alpine compressional thrust planes, or late Alpine extensional brittle-ductile and brittle shear zones (Ivanov, 1988; Burg et al., 1990; Ivanov et al., 2000). The deposits of the CRD comprise epithermal to mesothermal Pb-Zn veins, stockworks, and metasomatic replacements of marbles as the most economic orebodies. Almost all orebodies are crosscutting the detachment, which clearly indicate that mineralization is younger than the tectonic events in the region. In general, the ore fields exhibit similar characteristics of mineralization and a relatively uniform and compositionally simple mineral association. The main minerals are quartz, galena, sphalerite, pyrite, chalcopyrite and calcite (Rohrmeier et al, 2013 and references therein).

Laki district geology

The Laki ore field situated to the south from the town of Laki, on the northern slope of the CRD and western border of the Eastern Rhodope Paleogene Depression. The district is made up of metamorphic rocks of Arda and Asenitsa tectonic units. Vein-hosted, polymetallic mineralization is hosted along four linear elongated fault zones, which consist of steeply dipping NNE-SSW faults, up to 7 km in length. Metasomatic replacement ore-bodies occur when the polymetallic feeder veins cross-cut marble horizons, resulting in the formation of large, irregular mineralized bodies, found up to 140 m away from the ore bearing veins (Stoynova, 1988). **Five paragenetic stages** have been described by (Stoynova, 1988): (1) skarn, (2) epidote-quartz-pyrite, (3) quartz-sphalerite-galena, (4) dolomite-sphalerite, and (5) quartz-calcite.

Madan district geology

Madan ore field is located in the south-western part of the CRD (Fig. 1). Host rocks in the area of the ore field belong to Arda and Madan tectonic units. The larger deposits are related to six subparallel NNW-trending fault zones with lengths up to 15 km and more. The ore bodies are of three types – veins, carbonate replacement bodies and stockworks (Kostova et al., 2004). According to Ivanov et al. (2000), 6 paragenetic stages can be distinguished: (1) quartz–pyrite, (2) quartz–galena, (3) quartz–galena–sphalerite, (4) rhodochrosite–dolomite–manganocalcite, (5) quartz–arsenopyrite ± sulphosalts, and (6) manganocalcite–calcite, not all of which are present in all parts of all mines (Ivanov et al., 2000).

The temperature distribution with depth from fluid inclusion analyses shows that they were associated with different stages of mineralization. Kostova et al. (2004) characterized three paragenetic types of quartz (Q1, Q2 and Q3) for the evolution of ore forming fluids (Fig. 2 and 4). The early quartz–pyrite association formed when the hydrothermal system was still heating up (Q1). The somewhat later quartz–galena–sphalerite main ore stage was deposited during the thermal peak under hot hydrostatic head conditions with a temperature-depth distribution representing the fluid's boiling curve (Q2), and post-sulphide quartz formed after the thermal peak (Q3).

2. Geochronology

The geochronological story of the CRD is presented on the Fig. 3. The ore formation was the last stage of this story. The epithermal ore deposits were generated 31-29 m.y ago within 1 km from surface, 2 m.y. after upper-crustal magmatism by larger-scale hydrothermal fluid circulation. This process was potentially driven by high heat flow following core complex formation and rapid denudation of the dome in the final stages of the orogenic collapse (Kostova et al., 2004).

At the lithosphere scale, the thermal to hydrothermal history of the CRD was probably driven by asthenospheric upwelling, following the southward retreat of a Mesozoic slab that had driven the porphyry Cu-Au systems of southeastern Europe during the Late Cretaceous (Rohrmeier et al, 2013 and references therein).

3. Hydrodynamic model and ore metal solubilities of Madan ore field

General trend of hydrothermal convection around the pluton as a function of host rock permeability was proposed by Hayba and Ingebritsen (1997). Above the pluton, the hydrothermal system first establishes a steep thermal gradient until after about 6000 years the system has developed a temperature-depth profile that corresponds to hot hydrostatic head conditions. This remains largely unchanged until, about 10’000 years after intrusion emplacement, the lower part of the system begins to cool faster than the upper part because the laterally recharging cold fluid cannot anymore be heated sufficiently by the cooled pluton. As a result, a negative temperature slope develops while there is a general cooling trend in the overall system.

The trends in the Yuzhna Petrovitsa fluid inclusion homogenization temperatures quantitatively match the general trends predicted by Hayba and Ingebritsen (1997) at a depth interval of around 1200–700 m (Fig. 4). The Q1 data match the “heating up” phase about 4000–5000 years after intrusion, Q2 records the period between about 5000 and 8000–9000 years under hot hydrostatic head conditions in a boiling fluid column, and Q3 represents the situation about 10’000 years after intrusion.

The solubility of ore metal is mainly controlled by chloride activity, pH value and the amount of total reduced sulphur. In general, high salinity, low pH and low molality of total reduced sulphur (m_{Stot}) favour the solubility (see reactions below); of which salinity has the largest influence since solubility runs with power n (typically, n= 3 for Pb and n=4 for Zn under the conditions of interest; Seward, 1984; Ruaya and Seward, 1986).

The solubility of galena and sphalerite from hydrothermal solutions is controlled by following reactions:

$$PbS + nCl^- + 2H^+ = PbCl_n^{2-n} + H_2S \quad (1)$$
$$ZnS + nCl^- + 2H^+ = ZnCl_n^{2-n} + H_2S \quad (2)$$

Since Pb and Zn concentrations of fluids was obtained by LA-ICPMS analysis, total chloride concentrations was also obtained from fluid inclusion results, the pH and m_{Stot} remain unknown but can be constrained from ore mineral and alteration assemblages. Based on the study of Barrett and Anderson (1988), we can conclude that, during Q2 stage, the observed low concentration of Pb and Zn is the result of galena and sphalerite precipitation by cooling over 400m interval. Moreover, the precipitation mechanism of galena and sphalerite could be resulted in CO2 loss to the vapour phase and cause fluid boiling and subsequent increase of pH. Kostova et al. (2004) estimated the maximum pH at which the observed solubilities were possible at 310 °C would be around 5.2. Therefore, a slightly acidic fluid with pH below that of the K-feldspar–muscovite–quartz is in agreement with the field observation that all feldspar in rock fragments within the veins or in the wall rock immediately adjacent to the vein is altered to white mica.

On the other hand, inclusions in Q3 quartz post-date the main ore stage and show higher salinity which dramatically increase the solubility of the ore metals (approximately 6 times for galena and 11 times for sphalerite). The increase of solubility due to slight salinity increase in the late fluids is in excellent agreement with the dissolution textures frequently seen on galena crystals at Madan.

References

Burg, J.P., Ivanov, Z., Ricou, L.E., Dimor, D., and Klain, L., 1990, Implications of shear-sense criteria for the tectonic evolution of the Central Rhodope Massif, southern Bulgaria: Geology, v. 18, p. 451–454.

Hayba, D.O. and Ingebritsen, S.E., 1997, Multiphase groundwater flow near cooling plutons: J. Geophys. Res. 102, B6, 12235–12252.

Ivanov, Z., 1988, Apreçu général sur l'évolution géologique et structurale du massif des Rhodopes dans le cadre des Balkanides: Société Géologique de France, Bulletin, v. 8, p. 227–240.

Ivanov, Z., Dimov, D., Dobrev, S., Kolkovski, B., and Sarov, S., 2000, Structure, alpine evolution and mineralizations of the central Rhodopes area (south Bulgaria): ABCD-GEODE 2000 Workshop, Borovets, Bulgaria: Bulgaria, University Press "St. Kliment Ohridski," p. 1–50.

Rohrmeier, K.M., von Quadt, A., Driesner, T., Heinrich, C.A., Handler, R., Ovtcharova, M., Ivanov, Z., Petrov, P.,

Sarov, St., and Peytcheva, I., 2013, Post-orogenic extension and hydrothermal ore formation: high-precision geochronology of the Central Rhodopian Metamorphic Core Complex (Bulgaria-Greece): Economic Geology, v. 108, p. 691-718.

Ruaya, J.R. and Seward, T.M., 1986, The stability of chlorozinc (II) complexes in hydrothermal solution up to 350°C: Geochim. Cosmochim. Acta 50, 651–661.

Seward, T.M., 1984, The formation of lead (II) chlorids complexes to 300°C: A spectrophotometric study: Geochim. Cosmochim. Acta 48, 212–134.

Stoynova, M., 1988, Laky ore field: Lead-zinc deposits in Bulgaria, S., Technika, 79-90 (in Bulgarian).

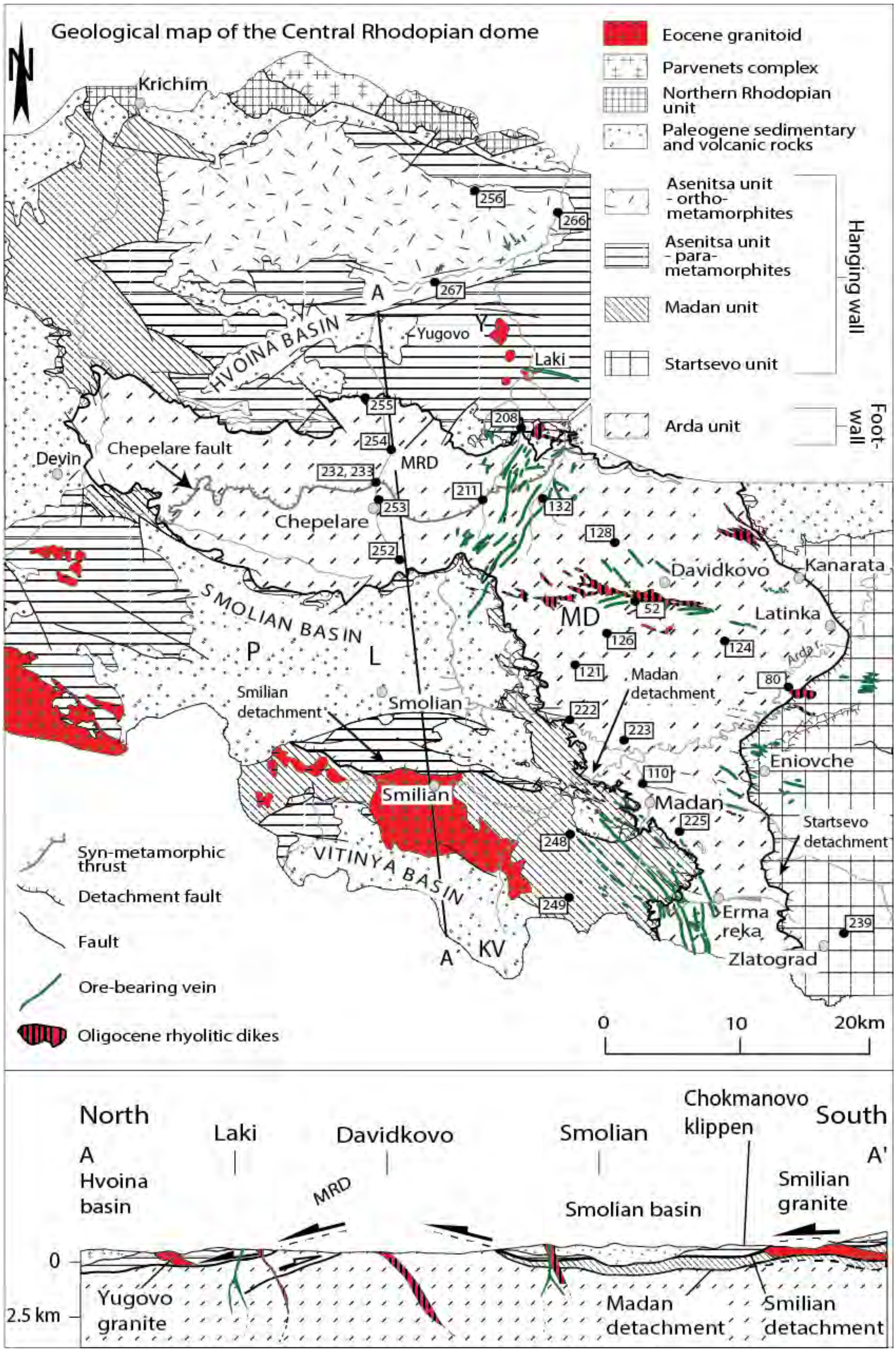

Figure 1: Geologic map and N-S cross section (A-A') of the Central Rhodope dome, modified after Burg et al. (1990) and Ivanov et al. (2000), displaying sample locations (Rohrmeier et al., 2013).

A-A' – line of cross section, B-B' – line of the cross section, shown in Fig. 2.

KV = Kotili-Vitinya ignimbrites, L = Levocevo caldera, MD = Momchilovtsi-Davidkovo dike swarm, MRD = Middle Rhodopian detachment fault, P = Perelik ignimbrites, Y = Yugovo granite, Z = Zagrazden dike swarm

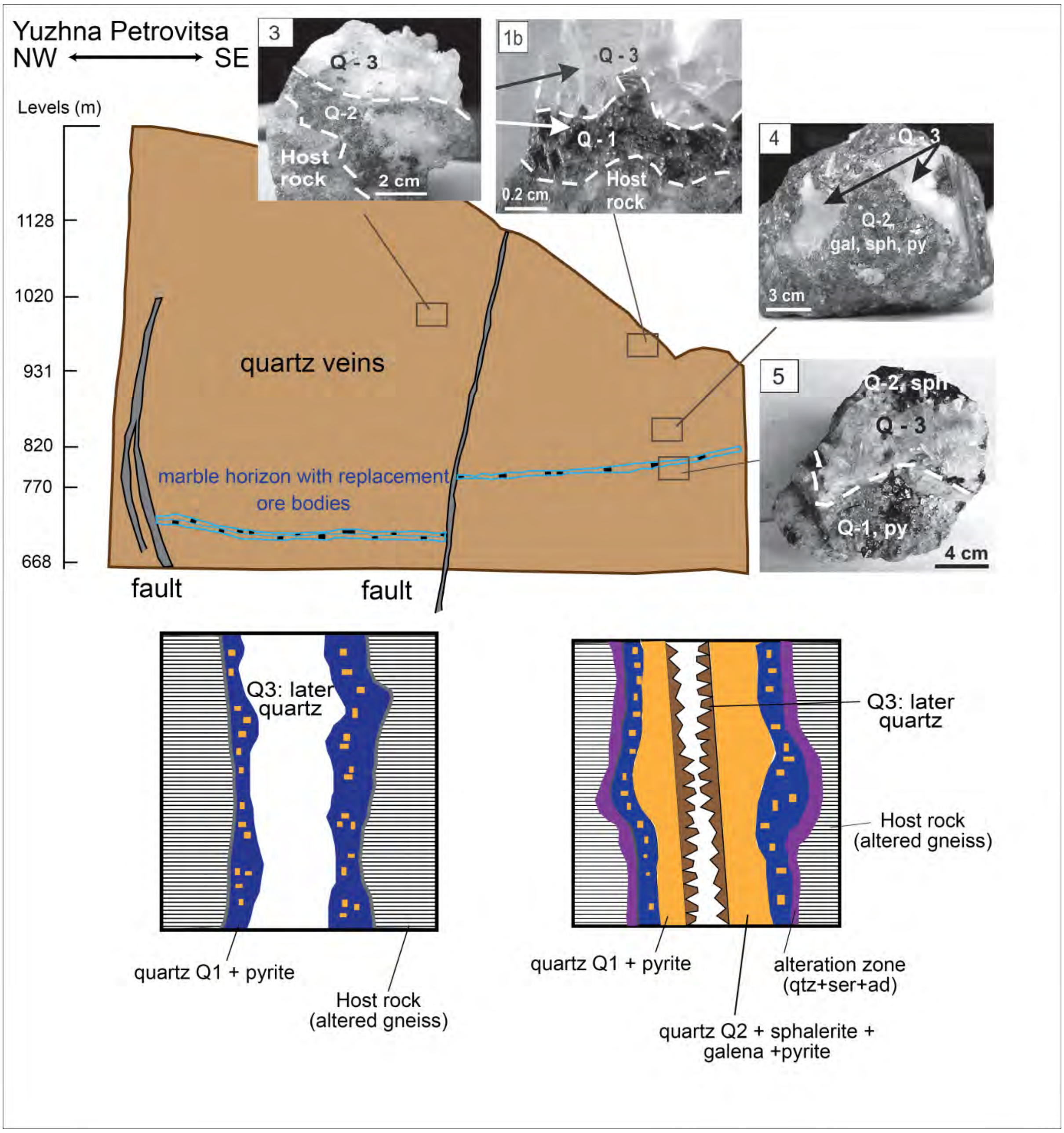

Figure 2: Schematic cross section through the Yuzhna Petrovitsa mine, and the schematic drawing of the space relation of host rock and different paragenetic stages of veins (Q1, Q2 and Q3).

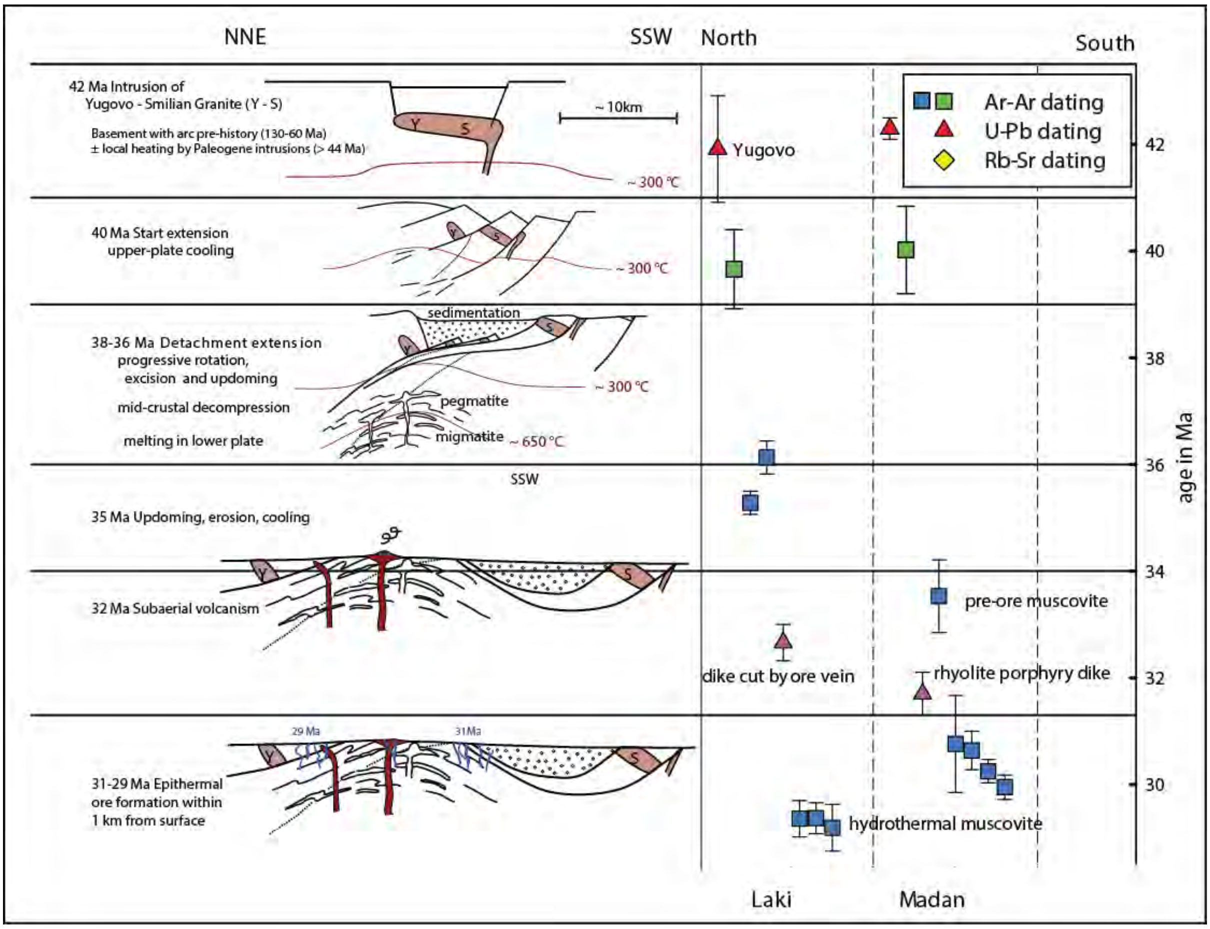

Figure 3: Schematic evolution of the Madan core complex during progressive extension leading up to hydrothermal Pb-Zn ore formation, interpreted from geology and integrated geochronological data, combined with a summary of geochronological data for Madan and Laki ore fields defining peak metamorphism, dome formation, and epithermal Pb-Zn mineralization in the CRD, all occurring within a time span of about 10 m.y. (modified from Rohrmeier et al., 2013)

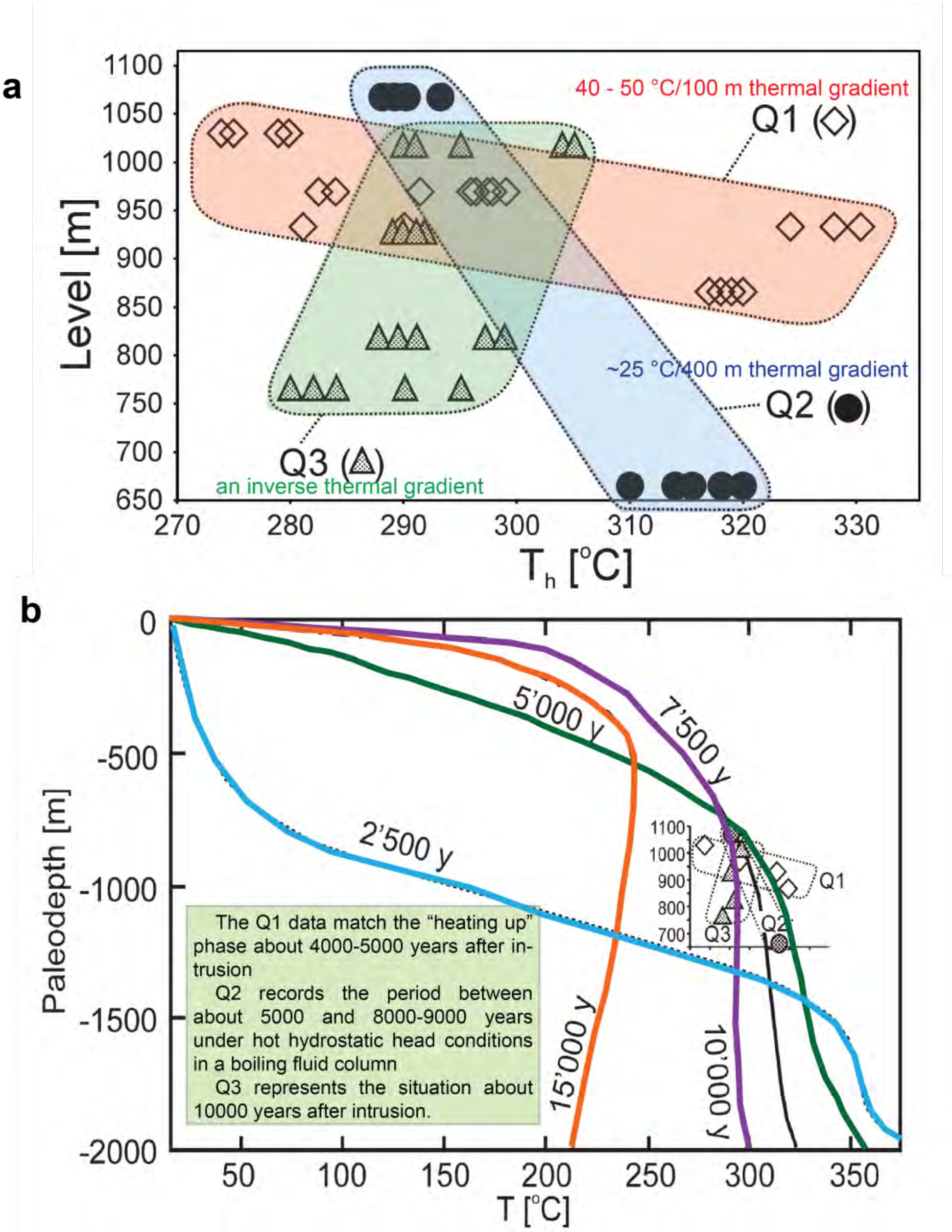

Figure 4a: Fluid inclusion homogenization temperatures vs. mine level for three quartz stages. Temperature distribution showed nearly linear trend with a gradient of about 40 -50 °C/ 100m for Q1; an upward temperature drop by 25 C by 400 m depth difference; whereas Q3 indicates an inverse thermal gradient.

Figure 4b: Hydrodynamic model of fluid flow above a cooling pluton. The hydrothermal convection around the pluton was calculated as a function of host rock permeability of 10 -15 m^2 (Hayba and Ingebritsen (1997). Figures are modified from Kostova et al. (2004).

Chernomoretz – Miarolitic cavities and fluid exsolution

Magmatic fluids are an essential part of magmatic-hydrothermal ore systems because they carry metals and their ligands. Based on publications by Candela (1997), Shinohara et al. (1995) and Hedenquist & Lowenstern (1994), it will be summarized (i) how magmatic fluids exsolve and separate from the magma and (ii) how they express themselves, with focus on miarolitic cavities.

Evidence for fluid separation comprises e.g. immense hydrothermal alteration, fluid and melt inclusions with elevated volatile components, volcanic degassing of SO2, H2O, CO2 + Cu, Au, etc., interlayered unidirectional solidification textures, and miarolitic cavities. The latter are voids in plutonic rocks surrounded by super-solidus minerals that formed by external nucleation on a bounding (liquid) surface (Figure 1 and 2). They typically occur in the upper parts of granite bodies. Flux-rich pegmatites can also produce miarolitic cavities, the cavities are the last part of the pegmatite to crystallize. They are most likely preserved if they form at a shallow level and if the melt is partially quenched. As bubble size and crystal size approach each other, the probability of preserving the bubble becomes greater. The bubbles can grow by diffusion, decompression and coalescence. Usually there exists a gradient in crystal size from the granite (mm scale) to the crystals in the cavity (cm scale). Miarolitic cavities are thus closely related to pegmatites. The crystals grow in the direction of the miarolitic cavities. Common minerals in pegmatites and miarolitic cavities comprise quartz, mica, alkali feldspar and albite (which crystallize at the eutectic), as well as rare minerals such as tourmaline, beryl and topaz that contain highly incompatible elements. The minerals often testify of crystallization continuing to low temperatures relative to normal magmatic temperatures. The crystals in miarolitic cavities commonly have a euhedral shape, possess shiny faces and show multiple fractures. Another typical feature is that the crystals in the miarolitic cavities are gem-clear. This is due to rapid diffusion and the high flux content of the fluid that crystallize the minerals. The rapid diffusion ensures a more uniform growth of the crystal faces. The fluid is a very dense hydrous silicate gel. Miarolitic cavities can be mined for the gemmology industry. Etched, skeletal or graphic crystals may also be present. The composition from the host rock to the centre of the miarolitic cavity may over a cm-scale, which is relatively abrupt. The cavity may be filled with clay and may contain zeolites deposited on the other minerals. The clays represent the remnants of the dense hydrous silicate gel. Fluids that don’t crystallize might migrate in the adjacent rock and cause hydrothermal alteration.

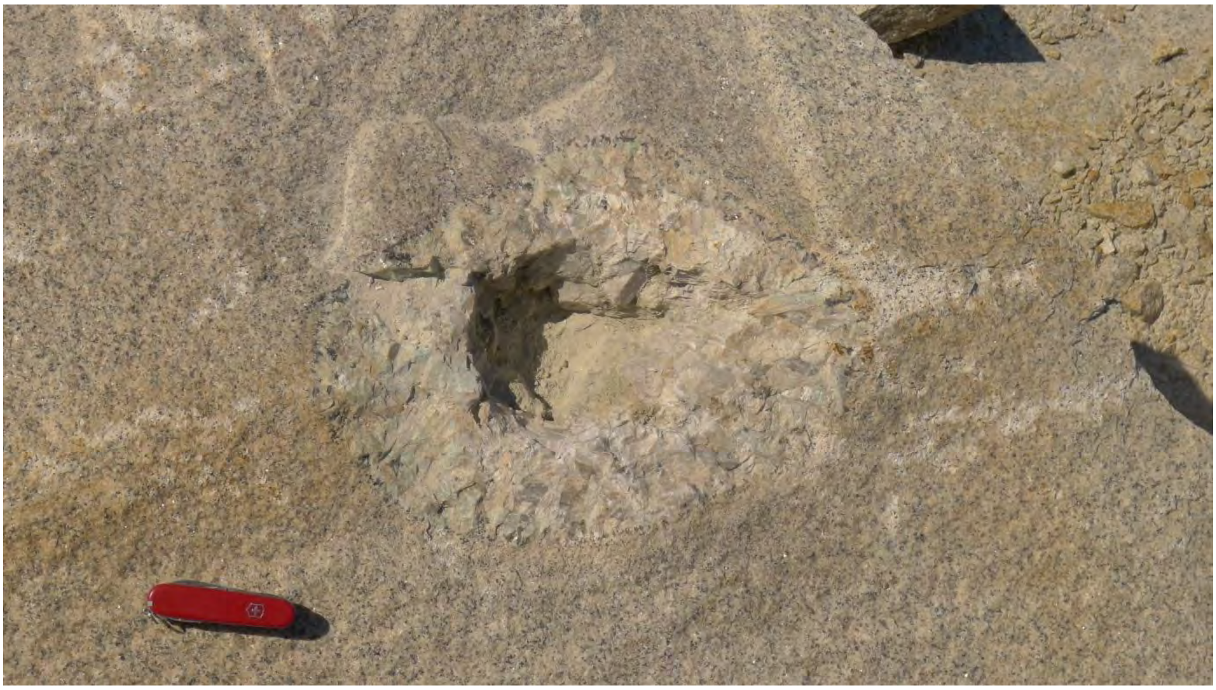

Figure 9: Miarolitic cavity in Rapakivi granite, Finland (photo by Stoeff)

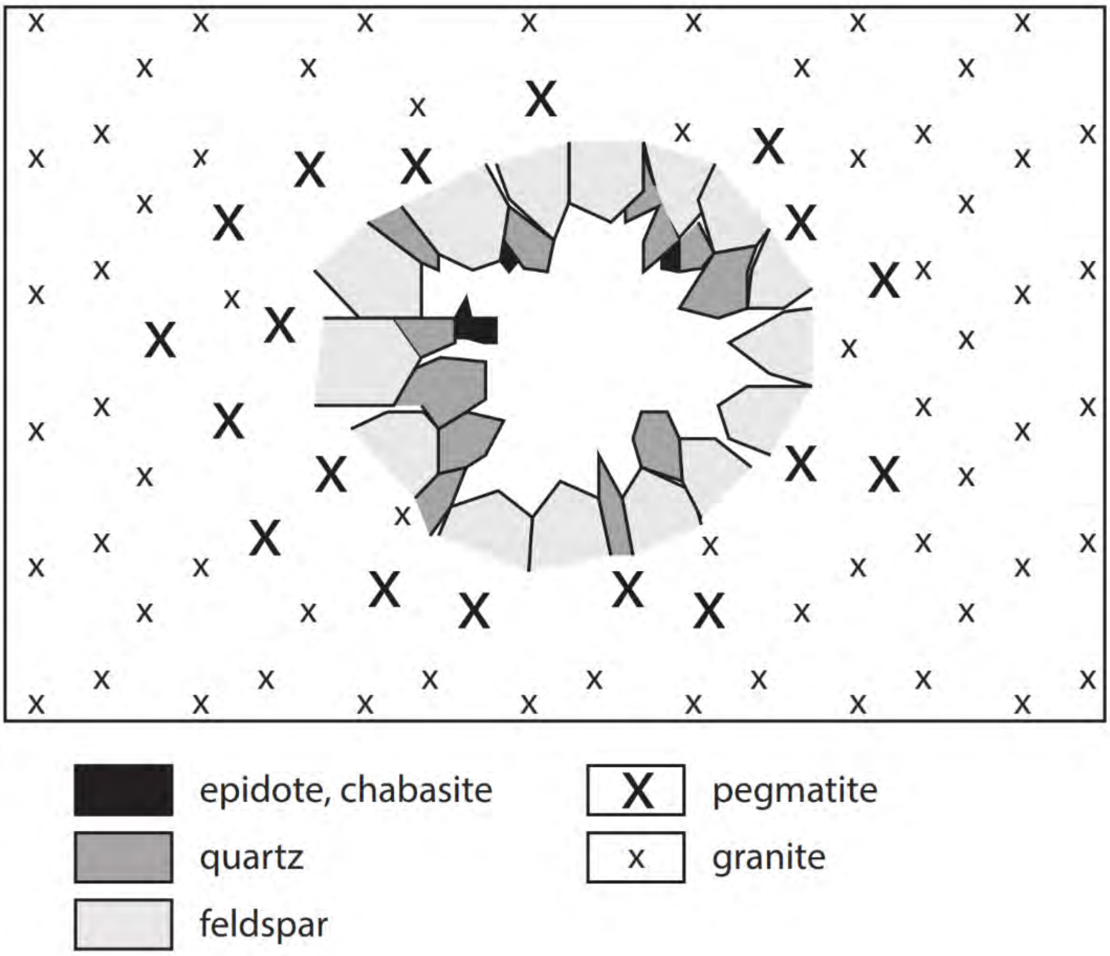

Figure 10: Sketch of miarolitic cavity from Chernomoretz, loosely based on exhibit displayed in Focus Terra. Increasing grain size towards the void, rather smooth transition from granite to pegmatite and euhedral crystals on the cavity's wall.

Two processes exist that cause fluid saturation and exsolution. First boiling is due to decompression, which can be caused by magma ascent or magma chamber failure. At first boiling the load pressure decreases. Second boiling is caused by crystallization of dominantly anhydrous phases which is mostly due to temperature decrease. It leads to the increase of vapour pressure in the magma. If the sum of vapour pressures is equal to the load pressure, bubbles can nucleate. The drop in water concentration in the melt due to first boiling can cause undercooling due to increase of the solidus temperature. Contrary to intuition, the separation of fluid from the magma during second boiling results in a drop of the solidus temperature. This is because the CO1 rich fluids are exsolved first due to the lower solubility of CO_2. This process leads to an increase of the water activity in the magma. Formation of bubbles can increase the viscosity of the melt. The volume will increase due to the expansion of the fluids in the bubbles. This is partly the cause of a lower density of the bubbles compared to the melt. This lower density enables the bubbles to ascend faster than the magma.

The release of the volatile phase from the magma depends on saturation, melt and crystals, pressure, phase proportions, rate of magma ascent, cooling rate, etc. The volatiles can be transported through the magma by a) diffusion, b) buoyancy, c) permeable flow and d) convection. A) Diffusion will be important for the nucleation of the bubbles, but it is too slow to transport over long distances. B) Because of buoyancy, single bubbles may rise and can coalesce along the way. This could be a slow process in in a high viscosity melt or in strongly crystallized magma, but may also be facilitated by the presence of crystals and shear stress. C) The bubbles can form a network through which the fluid can percolate through advection. This is also called permeable flow. Interconnected miarolitic cavities may be evidence for this process. This will only be efficient at the very top, since the bubble/magma fractions are highest here. This means that it won't cause transport over great distances (>1km). D) The density increase of the melt due to fluid exsolution will cause convection in the magma. The bubble rich magma will rise and thus transport the volatiles to the top. There it will lose the bubbles. The resulting higher density magma will migrate downwards (Figure 3).

Metals are scavenged by the volatiles. This scavenging is most efficient if no crystallization of ligand- or metal-bearing phases occurs before volatile separation. Another factor that plays a role is the partition coefficient of the metals. The compatibility of the metals with either the fluid, melt or crystals depends on crystal structure, melt and fluid composition (e.g. possible ligands), oxidation state, temperature, and pressure. If crystallization of minerals with partition coefficients below one for a specific metal happened before fluid exsolution, the metal will be enriched in the melt (Figure 3).

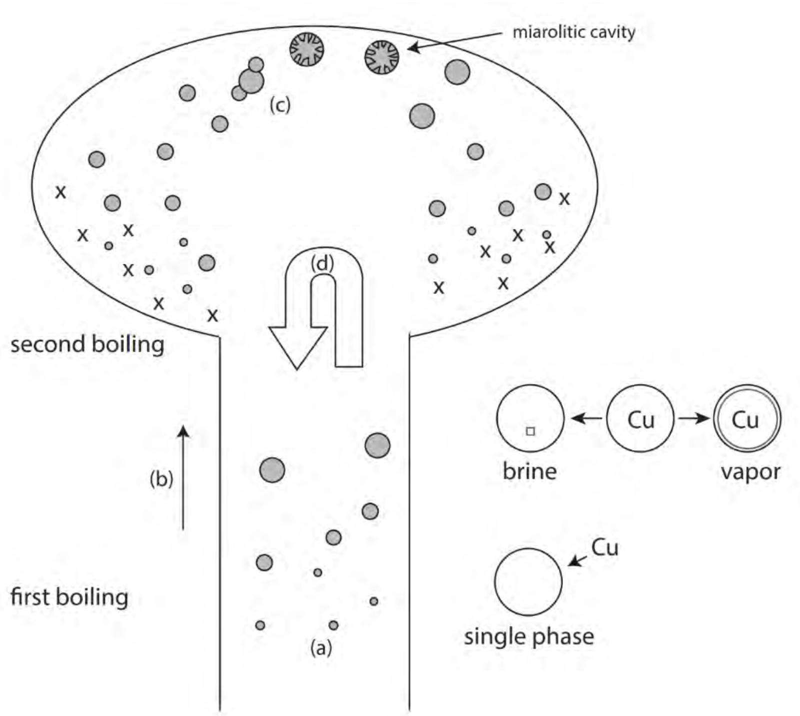

Figure 11: Representation of a magma conduit and chamber. First and second boiling are pictured. To the right the evolution in bubble composition is depicted.

Important ligands are chloride and sulphide. Depending on fluid composition, pressure and temperature, the fluid may separate into two fluid phases upon ascending. At intermediate depths and volatile concentrations the fluid normally separates into a dense brine and lighter vapour. Addition of CO2 increases the field of immiscibility. Important for the formation of the two phases is the initial chloride-water ratio, initial water content and pressure (Figure 4). The separation of fluid phases will result in a new partitioning of the metals between the vapour and the brine. The dynamics of transport of the denser brine will be different. The density contrast might result in gravitational stratification of magma, brine, and vapour. Because of the higher density of the brine compared to the vapour it may resist migration and stay dispersed, while the vapour may continue to rise and accumulate. The vapour and the brine will posses a different ligand composition and will thus produce different ores.

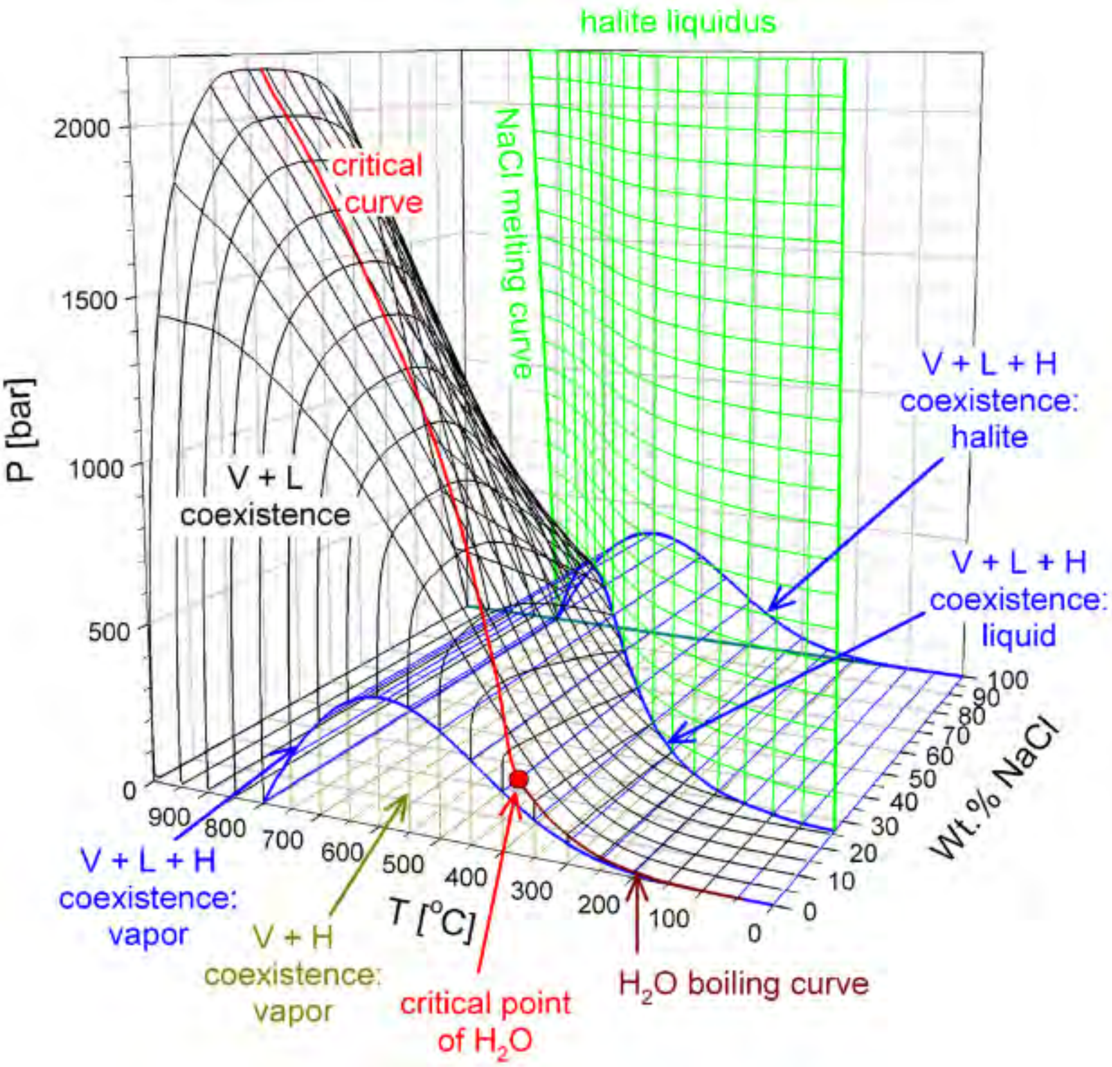

Figure 12: Phase diagram for H2O-NaCl systems from Driesner & Heinrich (2007) visualizes how a single-phase fluid can separate into two phases upon decompression and cooling.

References:

Candela, P. A. (1997). A review of shallow, ore-related granites: textures, volatiles, and ore metals. *Journal of petrology*, *38*(12), 1619-1633.

Driesner, T., & Heinrich, C. A. (2007). The system H 2 O–NaCl. Part I: Correlation formulae for phase relations in temperature–pressure–composition space from 0 to 1000° C, 0 to 5000bar, and 0 to 1 X NaCl. *Geochimica et Cosmochimica Acta*, *71*(20), 4880-4901.

Hedenquist, J. W., & Lowenstern, J. B. (1994). The role of magmas in the formation of hydrothermal ore deposits. *Nature*, *370*(6490), 519-527.

London, D. (2008). Pegmatites. Mineralogical association of Canada, Québec, 347.

Shinohara, H., Kazahaya, K., & Lowenstern, J. B. (1995). Volatile transport in a convecting magma column: Implications for porphyry Mo mineralization. *Geology*, *23*(12), 1091-1094.


Untitled Map
Write a description for your map.
Legend
Feature 1
Chelopech
Chelopech
Mirkovo
Google earth
900 m


Untitled Map
Write a description for your map.
Legend
Feature 1
Panagyurški kolonii
Google earth


Elshitsa
Untitled Map
Write a description for your map.


Untitled Map
Legend
Ruse
Ruse
Dobrich
Razgrad
Balchik
Montana
Pleven
Targoviste
Shumen
Varna
Vratsa
Vraca
Lovec
Bulgaria
Tarnovo
Gabrovo
Sofia-city
Sofia
Sofia
Sliven
Sliven
Pernik
Burgas
Burgas
Jambol
Stara Zagora
Stara Zagora
ustendil
Pazardzik
Pazardzhik
Plovdiv
Plovdiv
Blagoevgrad
Blagoevgrad
Haskovo
Haskovo
Kirklareli
Edirne
Kardzali
Smoljan
2850 Petrich
Çorlu
Edirne
Tekirdag


Untitled Map
Legend
Pravets
Novi Iskar
Boykovets
Etropole
Yamna
Lokorsko
Svetovrachene
Sofia
Buhovo
Gorno Kamartsi
Stargel
Yana
Sarantsi
Zlatitza
Chelopech
Chelopech
Mirkovo
Pirdop
Gorna Malina
Gorna Malina
Sofia
Elin Pelin
Kazichene
Chavdar
Lesnovo
Chavdar
Novi khan
Lozen
Pancharevo
Bistritsa
Kamenitsa
Vakarel
Dolni Pasarel
Zheleznitsa
Buzyakovtsi
Srebrinovo
Paunovo
Poibrene
Dolni Okol
Google earth

Untitled Map
Legend
Lozen
Novi khan
Kamenitsa
Panagyurski kolonii
Vakarel
Dolni Pasarel
Buzyakovtsi
Srebrinovo
Paunovo
Poibrene
Panagyurishte
Dolni Okol
Ihtiman
Ihtiman
Popi
Shiroki dol
Mirovo
Lesichovo
Gutsal
Samokov
Samokov
Gorno varshilo
Kalugerovo
Dolna banya
Kostenetz
gr. Kostenets
Vinogradets
Raduil
Vetren
Beli Iskar
Borovets
Govedartsi
Kostenets
Boshulya
Sestrimo
Belovo
Belovo
Septemvri
Septemvri
Google earth


Untitled Map
Sapareva banya
Sapareva Banya
Beli Iskar
Borovets
Dupnitza
Dupnica
Samoranovo
Govedartsi
Vaksevo
Boboshevo
Boboshevo
Rila
Rila
Pastra
Rilski manastir
Kocherinovo
Kocherinovo
sarvaritsa
Blagoevgrad
Blagoevgrad
Blagoevgrad
Selishte
Gorno Osenovo
Dobarsko
Tserovo
Dolno Osenovo
Belitsa
Dolno Draglishte
Belitza
Padesh
Gradevo
Bachevo


Untitled Map
Kocherinovo
Blagoevgrad
Blagoevgrad
Blagoevgrad
Delchevo
Delchevo
Gradevo
Simitli
Simitli
Trabotivishte
Pehchevo
Berovo
Municipality of Berovo
Kresna
Strumyani
Ploski
Sandanski
Sandanski
Petrich
2850 Petrich
Petrich
Novo Selo
Strumitsa
Velingrad
Yakoruda
Yakoruda
Belitsa
Belitza
Bachevo
Razlog
Eleshnitsa
Bansko
Sarni
Garmen
Satovcha
Gotse Delchev
Gotze Delchev
Hadzhidimovo
Hadjidimovo


Untitled Map
Parvenets
Peshtera
Perushtitza
Krichim
Krichim
Velingrad
Peshtera
Bratzigovo
Yakoruda
Yakoruda
Rakitovo
Rakitovo
Belitsa
Batak
Rodopi
Bachevo
Belitza
Razlog
Eleshnitsa
Bansko
Batak
Sarnitsa
Devin
Chepelare
Chepelare
Borino
Garmen
Dospat
Dospat
Satovcha
Smolyan
Gotse Delchev
Gotze Delchev
Hadzhidimovo
Hadjidimovo

Untitled Map
Legend
Laki
Zhenda
Chernoochene
Chepelare
Rani list
Padartsi
Penyovo
Davidkovo
Pamporovo
Momchilovtsi
Kardjali
Kardzali
Strazhevtsi
Banite
Kyosevo
Ardino
Veleshani
Smolyan
Momchilgrad
Srednogortsi
Kiselchovo
Enyovche
Madan
Djebel
Smilyan
Valchan
Rudozem
Ustren
Nedelino
Sredok
Sivino
Ogled
Krushev dol
Gorovo
Starovo
Plovdivtsi
Ostrovets
Preseka


Untitled Map
Mandra
Zhalti Bryag
Slavyanovo
Malak Izvor
Stambolovo
Zhenda
Chernoochene
Maslinovo
Varbovo
Oreshets
Dolno Botevo
Tankovo
Zvinitsa
Rani list
Chiflik
Strahil voyvoda
Padartsi
Penyovo
Bryagovets
Dolno Cherkovishte
Madjarovo
Kardjali
Kardzali
Strazhevtsi
Kyosevo
Veleshani
Momchilgrad
Gorna Kula
Djebel
Karamfil
Krumovgrad
Pelin
Bagriltsi
Zhelezino
Ustren
Konche
Tintyava
Kazak
Starovo
Golyama Chinka
Golyamo Kamenyane
Ostrovets
Siniger

Untitled Map
Legend
Tvarditsa
Tvarditza
Sliven
Karnobat
Kableshkovo
Nesebar
Straldzha Municipality
Straldzha
Kameno
Kameno
Troyanovo
Pomorie
Pomorie
Burgas
Burgas
Ravnets
Kamenovo
Kermen
Nova Zagora
Jambol
Chernomorets
Sozopol
Omarchevo
Tenevo
Tundja
Sredets
Zidarovo
Bistrets
Primorsko
Radnevo
Radnevo
Ovchi kladenets
Lozenets
Sredetz
Tzarevo
Elhovo
Bolyarovo
Opan
Galabovo
Galabovo
Elhovo
Ahto
Topolovgrad
Topolovgrad
Kofçaz
Simeonovgrad
Simeonovgrad
Malko Tarnovo
Malko Tarnovo
Kofçaz
Dereköy
Harmanli
Harmanli
Hacıdanişment
Demirköy
Lalapaşa
Demirköy
Lalapaşa
Elena
Lyubimets
Lyubimets
Süloğlu
Süloğlu
Kırklareli
Kırklareli
Üsküp
Kırklareli
Yenice
Svilengrad
Kapitan Andreevo
Edirne
Edirne
İnece
İskender
Pinarhisar
Pinarhisar
Vize
Madjarovo
Havsa
Havsa
Google Earth

Untitled Map
Write a description for your map.
Legend
Feature 1
Perunika
Pelin
Krumovgrad
Krumovgrad
Polkovnik Zhelyazovo
Slivarka
Guliyka
Edrino
Google earth


Untitled Map
Legend
Feature 1
Malka Arda
Banite
Banite
Kupen
Levochevo
Tikale
Katranitsa
Selishte
Vehtino
Leshtak
Leska
Fatovo
Srednogortsi
Ravnil
Kokortsi
Boevo
Lovtsi
Madan
Mitovska
Dobreva cheresha
Bukovo
Smilyan
Maglishta
Tankoto
Madan
Zmievo
Byala reka
Sharenska
Google earth

Untitled Map
Legend
Tsaparevo
Suvi Laki
Valkovo
Sandanski
Lyubovka
Igralishte
Krandzhilitsa
Struma
Sklave
Drenovo
Gorno Spanch
Ribnik
Levunovo
Kalimantsi
Novo Konomladi
Dolene
Dolna Ribnitsa
Municipality of Novo Selo
Petrich
Kavrakirovo
Dolno Spanchevo
Novo Selo
Topolnitsa
2850 Petrich
Petrich
Novo Konjarevo
Kulata
Koleshino
Skrat
Yavornitsa
Belasitsa
Ano Poroia
Neo Petritsi

Untitled Map
Write a description for your map.
Legend
Feature 1
Krandzhilitsa
Hamzali
Drvosh
Bosilovo
Ilovitsa
Barbarevo
Stinik
Volno
Churilovo
Dolene
Vishlene
Turnovo
Sushitsa
Municipality of Novo Selo
Borovichene
Novo Selo
Samuilovo
Novo Konjarevo
Strumeshnitsa
Koleshino
Gabrovo
Mokrievo
Smolari
Gabrene
Skrat
Yavornitsa
Google earth